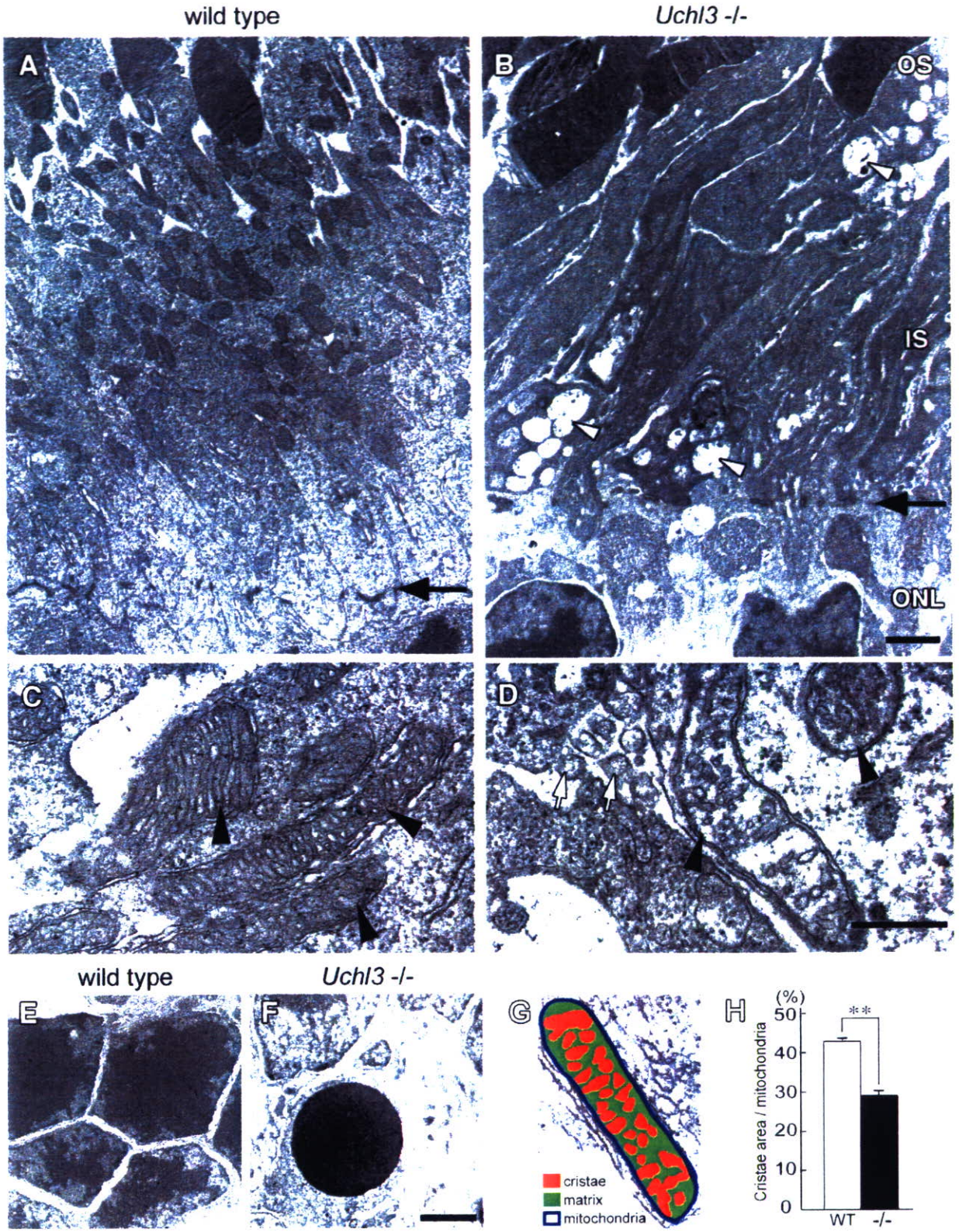

Figure 4. Ultrastructure of the outer retina in wild-type (**A**, **C**, and **E**) and *Uchl3*-deficient mice (**B**, **D**, and **F**) at 3w of age. **A** and **B:** Inner segment of mutant retina is shrunken associated with vacuolar changes (**arrowheads** in **B**). **Arrows** in **A** and **B** indicate outer limiting membrane. **C** and **D:** Subsets of mitochondria at the inner segment in *Uchl3*-deficient mice are swollen with decreased cristae (**arrowheads** in **D**) compared with that of wild-type (**arrowheads** in **C**). Groups of small round-to-oval shaped structures are occasionally seen in degenerated inner segment (**white arrows** in **D**). **E** and **F:** Outer nuclear layer of wild-type (**E**) and *Uchl3*-deficient (**F**) mice. Chromatin condensation of photoreceptor cells is observed in mutant mice (**F**). **G** and **H:** Morphometric analysis of mitochondria was performed with the percentage of cristae area (**G**; **red**) against mitochondrial area ($n = 50$ for each genotype). Cristae area in the inner segment is significantly decreased in mutant retina (**H**, $-/-$, **black bar**) compared with that in wild-type (**H**, WT, **white bar**). Each value represents the mean ± SE ($^{**}P < 0.01$). OS, outer segment; IS, inner segment; ONL, outer nuclear layer. Scale bars = 1 μm (**A** and **B**), 500 nm (**C** and **D**), and 1 μm (**E** and **F**).

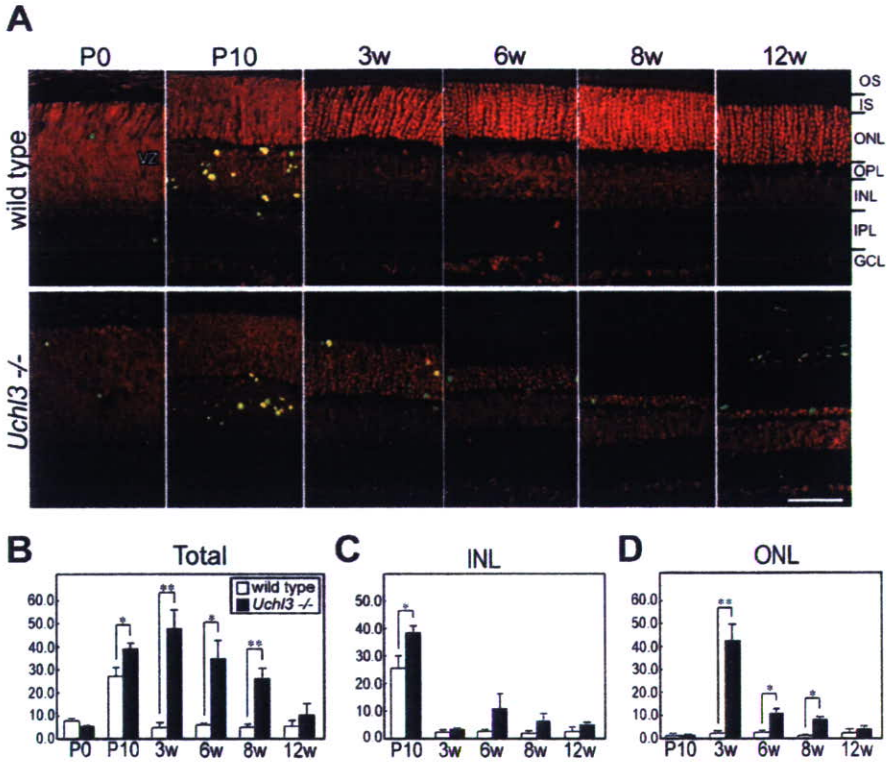

Figure 5. TUNEL analysis in wild-type and *Uchl3*-deficient mice at different ages. **A:** TUNEL staining in fluorescent microscopy shows that TUNEL-positive cells (**green**) are observed at the ventricular zone at P0 as well as at the inner nuclear layer at P10 in both genotypes. After 3w of age, TUNEL-positive cells are found in the outer nuclear layer in *Uchl3*-deficient mice. All sections are counterstained with propidium iodide (**red**). **B–D:** Number of TUNEL-positive cells in mutant mice (*Uchl3*$^{-/-}$; **black bar**) is significantly increased compared with those in wild-type (wild-type; **white bar**) at P10, 3w, 6w, and 8w (**B**). Increased number of TUNEL-positive cells in mutant mice at P10 correspond to apoptosis in the inner nuclear layer (**C**), whereas that in 3w, 6w, and 8w is reflected to apoptosis in the outer nuclear layer (**D**). VZ, ventricular zone; OS, outer segment; IS, inner segment; ONL, outer nuclear layer; OPL, outer plexiform layer; INL, inner nuclear layer; IPL, inner plexiform layer; GCL, ganglion cell layer. Scale bar = 20 μm (**A**). Each value in **B–D** represents the mean ± SE (*$P < 0.05$; **$P < 0.01$).

cient mice may be due to caspase-independent apoptotic pathway (Figure 7). Ubiquitin and Nedd-8, which are considered to be associated with UCH-L3 *in vitro*,[14,15] were expressed in the inner retina of both genotypes in a similar pattern as UCH-L1 (data not shown).

Discussion

This study demonstrates the unique localization of UCH-L3 to the photoreceptor inner segment that is abundantly populated with mitochondria after 3w of age in wild-type mice. The following features were found with regard to retinal degeneration in *Uchl3*-deficient mice. The retina showed no obvious morphological abnormalities during early postnatal development; however, progressive retinal degeneration was observed after 3w of age. The inner segment was originally perturbated with ultrastructural changes of mitochondria and increased expressions of markers for oxidative stress. The caspase-independent pathway was implicated during photoreceptor cell apoptosis. Thus, UCH-L3 may have a role in preventing mitochondrial oxidative stress-related apoptosis in photoreceptor cells.

Differential Localization of UCH-L1 and UCH-L3 in Murine Retina

The cellular distribution of UCH-L3 has not been studied except in the testis and epididymis, where UCH-L1 and UCH-L3 have distinct expression patterns.[25] In the present study, we found that UCH-L3 was enriched in the photoreceptor inner segment after 3w of age, whereas UCH-L1 was widely expressed in the inner retina. Photoreceptor cells are highly differentiated, and each segment has specific morphology and function; eg, inner segment contains abundant mitochondria,[27] and its oxygen consumption is considered to be high.[28] Meanwhile, expression of UCH-L1 at the inner retina was associated with that of ubiquitin and Nedd-8. Although *in vitro* studies indicate that UCH-L3 has de-neddylation activity,[14] UCH-L1 may be responsible for regulating expression level of ubiquitin and ubiquitin-like protein Nedd-8 in the retina. Because UCH-L1 expression in the retina was not altered in *Uchl3*-deficient mice, the function of UCH-L3 may not be compensated by UCH-L1. Our results indicate that UCH-L3 and UCH-L1 differ with regard to their localization and function in retina.

Mechanism of Photoreceptor Cell Death in the Uchl3-Deficient Mice

In our result, retinal apoptosis in *Uchl3*-deficient mice consisted of two different phases, during retinal development and after development. During the early postnatal development at P10, TUNEL-positive cells were observed in the inner nuclear layer of both genotypes, and the physiological apoptosis was slightly enhanced in the mutant retina. Because UCH-L3 was faintly expressed in the outer plexiform layer at P10 in wild-type mice, UCH-L3 may function during development. In the retinal development, the number of bipolar and Müller cell deaths reaches a peak at the postnatal days 8 to 11, which is associated with differentiation of the retina in

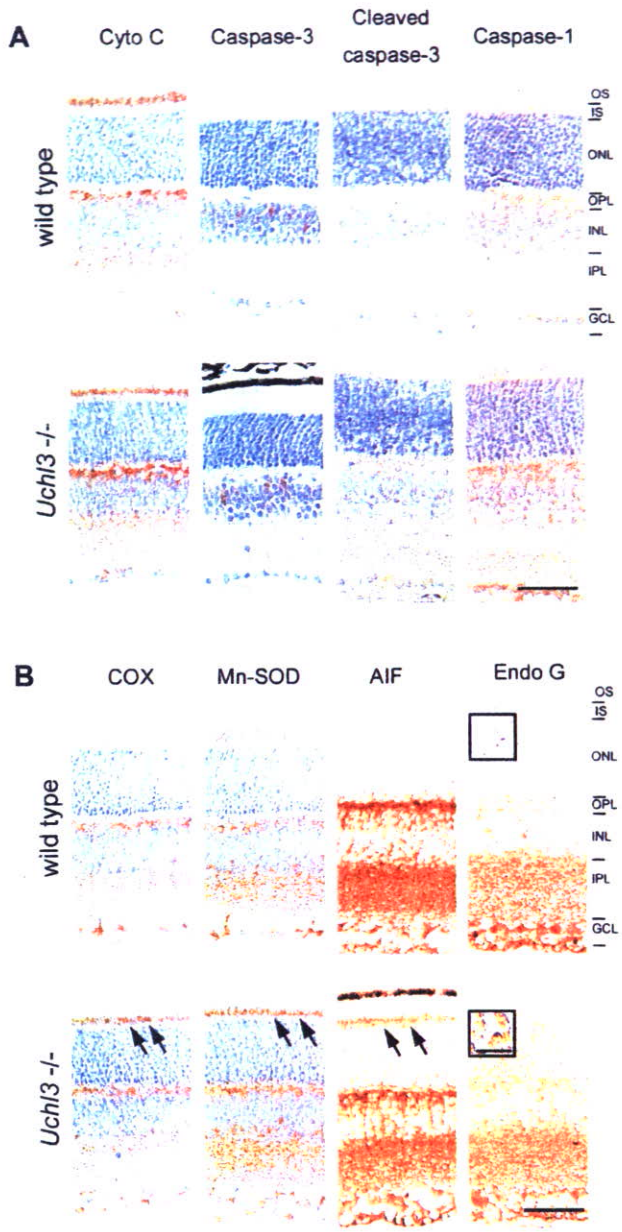

Figure 6. Immunohistochemical analysis of apoptosis- and oxidative stress-related molecules at 3w of age in wild-type and *Uchl3*-deficient mice. **A:** Expression of molecules relevant to the caspase-dependent pathway, including cytochrome *c* (Cyto C), caspase-3, cleaved caspase-3, and caspase-1, is unchanged between both genotypes. **B:** Increased immunoreactivities for oxidative stress markers, COX, Mn-SOD, and AIF, are observed in the inner segment of *Uchl3*-deficient mice (**arrows**). Translocation of Endo G to nuclei is found in the outer nuclear layer of *Uchl3*-deficient mice (**inset** in **B**). OS, outer segment; IS, inner segment; ONL, outer nuclear layer; OPL, outer plexiform layer; INL, inner nuclear layer; IPL, inner plexiform layer; GCL, ganglion cell layer. Scale bars = 50 μm (**A** and **B**); 10 μm (**inset** in **B**).

mice.[29] Therefore, loss of UCH-L3 may mildly promote the cell death of these cells.

After 3w of age, prominent and progressive photoreceptor cell apoptosis was disclosed in the outer nuclear layer of *Uchl3*-deficient mice. Under pathological conditions, several apoptotic pathways have been suggested in experimental retinal degeneration. Caspase-1 is predominantly associated with photoreceptor cell apoptosis in retinal degeneration of ischemia-reperfusion.[30] Light-induced retinal degeneration activates the parallel cascades, caspase-1[20] and caspase-independent apoptosis.[21] Oxidative stress leads to caspase-independent apoptosis in cultured cells.[31] Our results indicated that a caspase-independent pathway was activated during photoreceptor cell apoptosis in *Uchl3*-deficient mice, because immunohistochemical analysis revealed that activated caspase-3 and caspase-1 were not expressed in the degenerated retina. In addition, Endo G, a protein involved in the caspase-independent pathway, was expressed in the nuclei of the outer nuclear layer in *Uchl3*-deficient mice. Endo G is a mitochondria-specific nuclease that translocates to nuclei and serves as the DNase during a caspase-independent apoptosis.[32] Therefore, Endo G may be responsible for the DNA degradation that occurs during apoptosis in *Uchl3*-deficient mice. Expression of Endo G was slightly increased in the outer plexiform layer, inner nuclear layer, and inner plexiform layer of the *Uchl3*-deficient mice after 3w of age despite no significant UCH-L3 immunoreactivities in these layers. This result may reflect trans-synaptic secondary neuronal degeneration or glial changes of Müller cells.

AIF, another factor involved in caspase-independent apoptosis, was enriched in the inner segment; however, we did not observe translocation to nuclei for this protein. AIF is a mitochondrial flavoprotein that is a free radical scavenger of healthy cells.[33] During apoptotic induction, AIF translocates from mitochondria to nuclei.[33,34] It functions as a caspase-independent and PARP-1-dependent death effector that induces chromatin condensation and large-scale DNA fragmentation.[35] In our study, expression of AIF at the inner segment was associated with increased immunoreactivities of the oxidative stress markers, COX and Mn-SOD. Although it is unknown why AIF did not translocate to nuclei in the degenerated retina, increased immunoreactivity for AIF in the inner segment may indicate a reaction to oxidative stress. Because mouse eyes open 12 to 13 days after birth, light-induced oxidative stress may affect photoreceptor cell apoptosis in *Uchl3*-deficient mice after development. On the other hand, the retinal oxygen consumption increases under dark-adapted condition in the cat retina.[28,36] It may be interesting to study whether constant light or constant dark has any effect on the development of retinal degeneration in the *Uchl3*-deficient mice.

Uchl3-Deficient Mice as a Model of Retinal Degeneration with Mitochondrial Impairment

Apoptosis during retinal degeneration is observed in inherited diseases such as retinitis pigmentosa as well as in retinal diseases induced by a variety of stimuli, including hypoxia and oxidative stresses.[37,38] Several genetically engineered animal models of retinitis pigmentosa have been extensively investigated, including the RCS rat and *rd* mice. Retinal degeneration in the RCS rat was originally identified as an impairment of phagocytosis by pigmented epithelium due to mutation of receptor ty-

Table 1. Chronological Changes in Expression of Markers for Oxidative Stress and Caspase-Independent Apoptosis

	COX						Mn-SOD						AIF						Endo G					
	P0	P10	3w	6w	8w	12w	P0	P10	3w	6w	8w	12w	P0	P10	3w	6w	8w	12w	P0	P10	3w	6w	8w	12w
VZ*	−						−						−						−					
PR		−						−						−						−				
OS			−	−	nd	nd			−	−	nd	nd			−	−	nd	nd			−	−	nd	nd
IS			+	+	−	nd			+	+	+	nd			++	+	−	nd			−	−	−	nd
ONL		−	−	−	−	−		−	−	−	−	−		−	−	−	−	−		−	++§	+§	−	−
OPL		−	−	−	−	−		−	−	−	−	−		−	−	−	−	−		−	±§	±§	±	±
INL		−	−	−	−	−		−	−	−	−	−		−	−	−	−	−		−	±§	±§	−	−
IPL	−	−	−	−	−	−	−	−	−	−	−	−	−	−	−	−	−	−	−	−	−	−	±	±
GCL	−	−	−	−	−	−	−	−	−	−	−	−	−	−	−	−	−	−	−	−	−	−	−	−

*VZ, ventricular zone; PR, photoreceptor; OS, outer segment; IS, inner segment; ONL, outer nuclear layer; OPL, outer plexiform layer; INL, inner nuclear layer; IPL, inner plexiform layer; GCL, ganglion cell layer.
−, no change; ±, slight increase; +, mild increase; and ++, marked increase of immunoreactivity compared to that of wild type.
nd, not determined due to atrophic change.
§Nuclear staining.

rosine kinase (Mertk) with subsequent photoreceptor cell death occurring in a caspase-1- and -2-dependent manner.[39–42] *rd* mice have a recessive mutation in the rod cGMP phosphodiesterase β-subunit, and photoreceptor apoptosis occurs via a caspase-dependent mechanism.[43,44] Thus, these animal models of retinitis pigmentosa differ from *Uchl3*-deficient mice with regard to the mechanism of retinal degeneration.

The relationship between retinal degeneration and mitochondrial dysfunction has not been well studied except in Harlequin mice, which contain a mutation of AIF and exhibit progressive retinal degeneration.[45] We consider that the degeneration induced in the *Uchl3*-deficient mice is associated with mitochondrial dysfunction, because mitochondria in the inner segment of mutant retina exhibited morphological changes such as decreased cristae area. *Uchl3*-deficient mice reveal not only retinal degeneration but also muscle degeneration and mild growth retardation,[17] and thus the lack of UCH-L3 may affect general organs containing abundant mitochondria. Subtypes of mitochondrial diseases, such as chronic progressive external ophthalmoplegia and Kearns-Sayre syndrome, are caused by various mitochondrial DNA deletions and observed progressive ophthalmoplegia as well as retinitis pigmentosa.[46,47] Because UCH-L3 is predicted to be involved in the maintenance of mitochondrial function, *Uchl3*-deficient mice may be a model of disease that arises from mitochondrial impairment. Further studies are necessary to clarify the molecular mechanisms underlying retinal degeneration, as well as other organs in these animals.

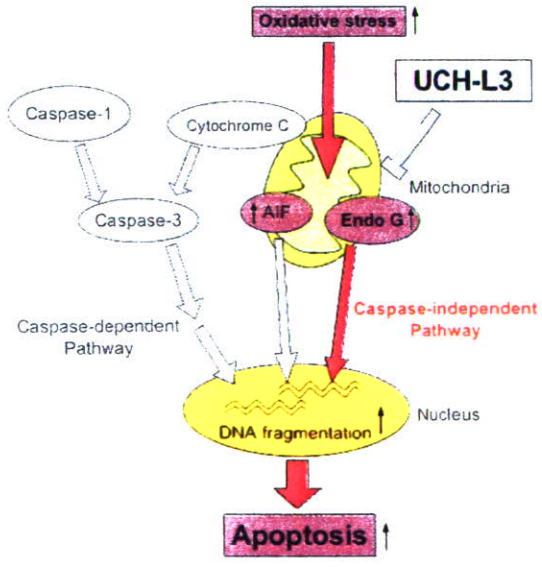

Figure 7. Function of UCH-L3 in apoptosis during retinal degeneration. Mitochondrial apoptosis is classified into caspase-dependent and caspase-independent pathways. Loss of UCH-L3 leads to oxidative stress-induced mitochondrial damage that causes translocation of Endo G from mitochondria to nuclei, resulting in caspase-independent apoptosis **Red arrows** are considered to be activated in *Uchl3*-deficient mice.

Acknowledgments

We thank Dr. S.M. Tilghman for providing *Uchl3*-deficient mice, Dr. K. Oyanagi, Dr. T. Harada, and Dr. K. Arima for their useful discussions, Ms. H. Fujita and Mr. D. Yamada for the breeding and care of the mice, and Mr. R. Debold, Ms. T. Matsuzawa, and Mr. N. Takagaki for editing the manuscript.

References

1. Amerik AY, Hochstrasser M: Mechanism and function of deubiquitinating enzymes. Biochim Biophys Acta 2004, 1695:189–207
2. Weissman AM: Themes and variations on ubiquitylation. Nat Rev Mol Cell Biol 2001, 2:169–178
3. Pickart CM, Eddins MJ: Ubiquitin: structures, functions, mechanisms. Biochim Biophys Acta 2004, 1695:55–72
4. Aguilar RC, Wendland B: Ubiquitin: not just for proteasomes anymore. Curr Opin Cell Biol 2003, 15:184–190
5. Wilkinson KD: Regulation of ubiquitin-dependent processes by deubiquitinating enzymes. FASEB J 1997, 11:1245–1256
6. Doran JF, Jackson P, Kynoch PA, Thompson RJ: Isolation of PGP 9.5, a new human neurone-specific protein detected by high-resolution two-dimensional electrophoresis. J Neurochem 1983, 40:1542–1547
7. Wilkinson KD, Lee KM, Deshpande S, Duerksen-Hughes P, Boss JM, Pohl J: The neuron-specific protein PGP 9.5 is a ubiquitin carboxyl-terminal hydrolase. Science 1989, 246:670–673
8. Osawa Y, Wang YL, Osaka H, Aoki S, Wada K: Cloning, expression, and mapping of a mouse gene, Uchl4, highly homologous to human and mouse Uchl3. Biochem Biophys Res Commun 2001, 283:627–633

9. Liu Y, Fallon L, Lashuel HA, Liu Z, Lansbury PT Jr,: The UCH-L1 gene encodes two opposing enzymatic activities that affect alpha-synuclein degradation and Parkinson's disease susceptibility. Cell 2002, 111:209–218
10. Leroy E, Boyer R, Auburger G, Leube B, Ulm G, Mezey E, Harta G, Brownstein MJ, Jonnalagada S, Chernova T, Dehejia A, Lavedan C, Gasser T, Steinbach PJ, Wilkinson KD, Polymeropoulos MH: The ubiquitin pathway in Parkinson's disease. Nature 1998, 395:451–452
11. Saigoh K, Wang YL, Suh JG, Yamanishi T, Sakai Y, Kiyosawa H, Harada T, Ichihara N, Wakana S, Kikuchi T, Wada K: Intragenic deletion in the gene encoding ubiquitin carboxy-terminal hydrolase in *gad* mice. Nat Genet 1999, 23:47–51
12. Wilkinson KD, Deshpande S, Larsen CN: Comparisons of neuronal (PGP 9.5) and non-neuronal ubiquitin C-terminal hydrolases. Biochem Soc Trans 1992, 20:631–637
13. Kurihara LJ, Semenova E, Levorse JM, Tilghman SM: Expression and functional analysis of *Uch-L3* during mouse development. Mol Cell Biol 2000, 20:2498–2504
14. Wada H, Kito K, Caskey LS, Yeh ET, Kamitani T: Cleavage of the C-terminus of NEDD8 by UCH-L3. Biochem Biophys Res Commun 1998, 251:688–692
15. Gan-Erdene T, Nagamalleswari K, Yin L, Wu K, Pan ZQ, Wilkinson KD: Identification and characterization of DEN1, a deneddylase of the ULP family. J Biol Chem 2003, 278:28892–28900
16. Kwon J, Wang YL, Setsuie R, Sekiguchi S, Sato Y, Sakurai M, Noda M, Aoki S, Yoshikawa Y, Wada K: Two closely related ubiquitin C-terminal hydrolase isozymes function as reciprocal modulators of germ cell apoptosis in cryptorchid testis. Am J Pathol 2004, 165:1367–1374
17. Semenova E, Wang X, Jablonski MM, Levorse J, Tilghman SM: An engineered 800 kilobase deletion of *Uchl3* and *Lmo7* on mouse chromosome 14 causes defects in viability, postnatal growth and degeneration of muscle and retina. Hum Mol Genet 2003, 12:1301–1312
18. Chang GQ, Hao Y, Wong F: Apoptosis: final common pathway of photoreceptor death in rd, rds, and rhodopsin mutant mice. Neuron 1993, 11:595–605
19. Cook B, Lewis GP, Fisher SK, Adler R: Apoptotic photoreceptor degeneration in experimental retinal detachment. Invest Ophthalmol Vis Sci 1995, 36:990–996
20. Grimm C, Wenzel A, Hafezi F, Remè CE: Gene expression in the mouse retina: the effect of damaging light. Mol Vis 2000, 6:252–260
21. Donovan M, Cotter TG: Caspase-independent photoreceptor apoptosis in vivo and differential expression of apoptotic protease activating factor-1 and caspase-3 during retinal development. Cell Death Differ 2002, 9:1220–1231
22. Osborne NN, Melena J, Chidlow G, Wood JP: A hypothesis to explain ganglion cell death caused by vascular insults at the optic nerve head: possible implication for the treatment of glaucoma. Br J Ophthalmol 2001, 85:1252–1259
23. Adler R, Curcio C, Hicks D, Price D, Wong F: Cell death in age-related macular degeneration. Mol Vis 1999, 5:31
24. Harada T, Harada C, Wang YL, Osaka H, Amanai K, Tanaka K, Takizawa S, Setsuie R, Sakurai M, Sato Y, Noda M, Wada K: Role of ubiquitin carboxy terminal hydrolase-L1 in neural cell apoptosis induced by ischemic retinal injury in vivo. Am J Pathol 2004, 164:59–64
25. Kwon J, Wang YL, Setsuie R, Sekiguchi S, Sakurai M, Sato Y, Lee WW, Ishii Y, Kyuwa S, Noda M, Wada K, Yoshikawa Y: Developmental regulation of ubiquitin C-terminal hydrolase isozyme expression during spermatogenesis in mice. Biol Reprod 2004, 71:515–521
26. Osaka H, Wang YL, Takada K, Takizawa S, Setsuie R, Li H, Sato Y, Nishikawa K, Sun YJ, Sakurai M, Harada T, Hara Y, Kimura I, Chiba S, Namikawa K, Kiyama H, Noda M, Aoki S, Wada K: Ubiquitin carboxy-terminal hydrolase L1 binds to and stabilizes monoubiquitin in neuron. Hum Mol Genet 2003, 12:1945–1958
27. De Robertis E: Electron microscope observations on the submicroscopic organization of the retinal rods. J Biophys Biochem Cytol 1956, 2:319–330
28. Linsenmeier RA, Braun RD: Oxygen distribution and consumption in the cat retina during normoxia and hypoxemia. J Gen Physiol 1992, 99:177–197
29. Young RW: Cell death during differentiation of the retina in the mouse. J Comp Neurol 1984, 229:362–373
30. Katai N, Yoshimura N: Apoptotic retinal neuronal death by ischemia-reperfusion is executed by two distinct caspase family proteases. Invest Ophthalmol Vis Sci 1999, 40:2697–2705
31. Carmody RJ, Cotter TG: Oxidative stress induces caspase-independent retinal apoptosis in vitro. Cell Death Differ 2000, 7:282–291
32. Li LY, Luo X, Wang X: Endonuclease G is an apoptotic DNase when released from mitochondria. Nature 2001, 412:95–99
33. Susin SA, Lorenzo HK, Zamzami N, Marzo I, Snow BE, Brothers GM, Mangion J, Jacotot E, Costantini P, Loeffler M, Larochette N, Goodlett DR, Aebersold R, Siderovski DP, Penninger JM, Kroemer G: Molecular characterization of mitochondrial apoptosis-inducing factor. Nature 1999, 397:441–446
34. Lorenzo HK, Susin SA, Penninger J, Kroemer G: Apoptosis inducing factor (AIF): a phylogenetically old, caspase-independent effector of cell death. Cell Death Differ 1999, 6:516–524
35. Yu SW, Wang H, Poitras MF, Coombs C, Bowers WJ, Federoff HJ, Poirier GG, Dawson TM, Dawson VL: Mediation of poly(ADP-ribose) polymerase-1-dependent cell death by apoptosis-inducing factor. Science 2002, 297:259–263
36. Linsenmeier RA: Effects of light and darkness on oxygen distribution and consumption in the cat retina. J Gen Physiol 1986, 88:521–542
37. Pacione LR, Szego MJ, Ikeda S, Nishina PM, McInnes RR: Progress toward understanding the genetic and biochemical mechanisms of inherited photoreceptor degenerations. Annu Rev Neurosci 2003, 26:657–700
38. Phelan JK, Bok D: A brief review of retinitis pigmentosa and the identified retinitis pigmentosa genes. Mol Vis 2000, 6:116–124
39. D'Cruz PM, Yasumura D, Weir J, Matthes MT, Abderrahim H, LaVail MM, Vollrath D: Mutation of the receptor tyrosine kinase gene Mertk in the retinal dystrophic RCS rat. Hum Mol Genet 2000, 9:645–651
40. Feng W, Yasumura D, Matthes MT, LaVail MM, Vollrath D: Mertk triggers uptake of photoreceptor outer segments during phagocytosis by cultured retinal pigment epithelial cells. J Biol Chem 2002, 277:17016–17022
41. Katai N, Kikuchi T, Shibuki H, Kuroiwa S, Arai J, Kurokawa T, Yoshimura N: Caspase-like proteases activated in apoptotic photoreceptors of Royal College of Surgeons rats. Invest Ophthalmol Vis Sci 1999, 40:1802–1807
42. Vollrath D, Feng W, Duncan JL, Yasumura D, D'Cruz PM, Chappelow A, Matthes MT, Kay MA, LaVail MM: Correction of the retinal dystrophy phenotype of the RCS rat by viral gene transfer of Mertk. Proc Natl Acad Sci USA 2001, 98:12584–12589
43. Jomary C, Neal MJ, Jones SE: Characterization of cell death pathways in murine retinal neurodegeneration implicates cytochrome c release, caspase activation, and bid cleavage. Mol Cell Neurosci 2001, 18:335–346
44. Lem J, Flannery JG, Li T, Applebury ML, Farber DB, Simon MI: Retinal degeneration is rescued in transgenic rd mice by expression of the cGMP phosphodiesterase β subunit. Proc Natl Acad Sci USA 1992, 89:4422–4426
45. Klein JA, Longo-Guess CM, Rossmann MP, Seburn KL, Hurd RE, Frankel WN, Bronson RT, Ackerman SL: The harlequin mouse mutation downregulates apoptosis-inducing factor. Nature 2002, 419:367–374
46. Land JM, Morgan-Hughes JA, Hargreaves I, Heales SJ: Mitochondrial disease: a historical, biochemical, and London perspective. Neurochem Res 2004, 29:483–491
47. Schmiedel J, Jackson S, Schäfer J, Reichmann H: Mitochondrial cytopathies. J Neurol 2003, 250:267–277

THE JOURNAL OF BIOLOGICAL CHEMISTRY VOL 281, NO. 41, pp. 30524–30533, October 13, 2006

Degradation of Amyotrophic Lateral Sclerosis-linked Mutant Cu,Zn-Superoxide Dismutase Proteins by Macroautophagy and the Proteasome*[S]

Received for publication, April 7, 2006, and in revised form, August 18, 2006 Published, JBC Papers in Press, August 18, 2006, DOI 10.1074/jbc.M603337200

Tomohiro Kabuta, Yasuyuki Suzuki, and Keiji Wada[1]

From the Department of Degenerative Neurological Diseases, National Institute of Neuroscience, National Center of Neurology and Psychiatry, Kodaira, Tokyo 187-8502, Japan

Mutations in the Cu,Zn-superoxide dismutase (SOD1) gene cause ~20% of familial cases of amyotrophic lateral sclerosis (fALS). Accumulating evidence indicates that a gain of toxic function of mutant SOD1 proteins is the cause of the disease. It has also been shown that the ubiquitin-proteasome pathway plays a role in the clearance and toxicity of mutant SOD1. In this study, we investigated the degradation pathways of wild-type and mutant SOD1 in neuronal and nonneuronal cells. We provide here the first evidence that wild-type and mutant SOD1 are degraded by macroautophagy as well as by the proteasome. Based on experiments with inhibitors of these degradation pathways, the contribution of macroautophagy to mutant SOD1 clearance is comparable with that of the proteasome pathway. Using assays that measure cell viability and cell death, we observed that under conditions where expression of mutant SOD1 alone does not induce toxicity, macroautophagy inhibition induced mutant SOD1-mediated cell death, indicating that macroautophagy reduces the toxicity of mutant SOD1 proteins. We therefore propose that both macroautophagy and the proteasome are important for the reduction of mutant SOD1-mediated neurotoxicity in fALS. Inhibition of macroautophagy also increased SOD1 levels in detergent-soluble and -insoluble fractions, suggesting that both detergent-soluble and -insoluble SOD1 are degraded by macroautophagy. These findings may provide further insights into the mechanisms of pathogenesis of fALS.

Amyotrophic lateral sclerosis (ALS)[2] is a neurodegenerative disease caused by selective loss of motor neurons (1, 2). Although most cases of ALS are sporadic, ~10% of ALS cases run in families. Dominant missense mutations in the gene that encodes the Cu,Zn-superoxide dismutase (SOD1) are responsible for 20% of familial ALS (fALS) cases (3). Mice overexpressing mutant SOD1 develop an ALS-like phenotype comparable with human ALS, whereas mice lacking SOD1 do not (4, 5). These findings have led to the conclusion that SOD1 mutants cause motor neuron degeneration by a toxic gain of function. Thus, studies of the degradation process of mutant SOD1 proteins could provide important insights into understanding the mechanisms that underlie the pathology of fALS, and possibly sporadic ALS, and into developing novel therapies for fALS by removing toxic species of mutant SOD1.

Cytoplasmic proteins are mainly degraded by two pathways, the ubiquitin-26 S proteasome pathway (6) and autophagy (7). Previous studies have shown that mutant SOD1 proteins are turned over more rapidly than wild-type SOD1, and a proteasome inhibitor increases the level of mutant SOD1 proteins (8, 9). Dorfin and NEDL1, two distinct ubiquitin ligases, ubiquitinate mutant but not wild-type SOD1 (10, 11). These observations suggest that mutant SOD1 is degraded by the ubiquitin-26 S proteasome pathway and that the increased turnover of mutant SOD1 is mediated in part by this pathway. On the other hand, the 20 S proteasome, a component of the 26 S proteasome, can degrade proteins without a requirement for ubiquitination (12, 13). A recent study has found that metal-free forms of wild-type and mutant SOD1 are degraded by the 20 S proteasome *in vitro* (14).

Autophagy is an intracellular process that results in the degradation of cytoplasmic components inside lysosomes. At least three forms of autophagy have been described in mammalian cells: macroautophagy, microautophagy, and chaperone-mediated autophagy (7). Macroautophagy is the major and the most well studied form of autophagy; this process begins with a sequestration step, in which cytosolic components are engulfed by a membrane sac called the isolation membrane. This membrane results in a double membrane structure called the autophagosome, which fuses with the lysosome. The inner membrane of the autophagosome and its protein and organelle contents are degraded by lysosomal hydrolases. Recent reports have demonstrated that macroautophagy plays an important role in preventing neurodegeneration in mice (15, 16). Although macroautophagy can be induced by starvation, this

* This work was supported by grants-in-aid for scientific research from the Japan Society for the Promotion of Science; a research grant in a priority area of research from the Ministry of Education, Culture, Sports, Science, and Technology, Japan; grants-in-aid for scientific research from the Ministry of Health, Labor and Welfare, Japan; and the Program for Promotion of Fundamental Studies in Health Sciences of the National Institute of Biomedical Innovation, Japan. The costs of publication of this article were defrayed in part by the payment of page charges. This article must therefore be hereby marked "*advertisement*" in accordance with 18 U.S.C. Section 1734 solely to indicate this fact.

[S] The on-line version of this article (available at http://www.jbc.org) contains supplemental Figs. S1–S6.

[1] To whom correspondence should be addressed: Dept. of Degenerative Neurological Diseases, National Institute of Neuroscience, National Center of Neurology and Psychiatry, 4-1-1 Ogawahigashi, Kodaira, Tokyo 187-8502, Japan. Tel.: 81-42-346-1715; Fax: 81-42-346-1745; E-mail: wada@ncnp.go.jp.

[2] The abbreviations used are: ALS, amyotrophic lateral sclerosis; fALS, familial ALS; SOD1, Cu,Zn-superoxide dismutase(s); 3-MA, 3-methyladenine; siRNA, short interfering RNA; EGFP, enhanced green fluorescent protein; HA, hemagglutinin; MTS, 3-(4,5-dimethylthiazol-2-yl)-5-(3-carboxymethoxyphenyl)-2-(4-sulfophenyl)-2H-tetrazolium.

pathway may take place constitutively in mammals (17). In cultured cells, inhibition of macroautophagy does not alter enhanced green fluorescent protein (EGFP) levels (18) or glyceraldehyde-3-phosphate dehydrogenase protein levels,[3] suggesting that not all cytosolic proteins are degraded by macroautophagy. To date, however, there have been no reports of macroautophagy in mutant SOD1 clearance.

In this study, we investigated the pathway by which human wild-type SOD1 and the A4V, G85R, and G93A SOD1 mutants are degraded in neuronal and nonneuronal cells. We show that wild-type and mutant SOD1 proteins are degraded by both the proteasomal pathway and macroautophagy. The experiments with inhibitors of these degradation pathways suggested that mutant SOD1 are degraded more rapidly than wild-type SOD1 in part by macroautophagy and that the contribution of macroautophagy to mutant SOD1 clearance is approximately equal to that of the proteasome pathway. Macroautophagy decreases mutant SOD1 protein levels in both nonionic detergent-soluble and -insoluble fractions. In addition, we provide data indicating that macroautophagy has a role in mutant SOD1-mediated cell death.

EXPERIMENTAL PROCEDURES

Plasmid Constructs—The expression plasmids pcDNA3-hSOD1 containing wild-type, A4V, G85R, and G93A mutant SOD1 were kindly donated by Ryosuke Takahashi (Kyoto University, Kyoto, Japan) and Makoto Urushitani (Laval University, Quebec, Canada) (19). To construct a plasmid expressing human wild-type SOD1 with the HA tag at the carboxyl terminus of SOD1, HA-tagged SOD1 fragments were amplified by PCR using wild-type SOD1 cDNA (Open Biosystems, Huntsville, AL) as the template. The PCR products were digested with XhoI and NotI and cloned into an XhoI-NotI-digested pCI-neo vector (Promega, Madison, WI). The primers used were 5′-AAAACTCGAGCCGCCAAGATGGCGACGAAGG-CCGTGTGCG-3′ and 5′-AAAAGCGGCCGCTTAAGCGTA-ATCTGGAACATCGTATGGGTATTGGGCGATCCCAATT-ACACCACA-3′. A plasmid expressing HA-tagged G93A SOD1 was generated using QuikChange site-directed mutagenesis kit (Stratagene, La Jolla, CA) according to the manufacturer's protocol. To construct a plasmid expressing fusion protein of green fluorescent protein and LC3, LC3 fragments were amplified by PCR using rat LC3 cDNA (Open Biosystems) as the template. The PCR products were digested with BglII and EcoRI and cloned into a BglII-EcoRI-digested pEGFP-C1 vector (Clontech). The primers used were 5′-ACTCAGATCTATGCCGTCCGAGAAGACCT-TCAAA-3′ and 5′-TGCAGAATTCTTACACAGCCAGTGCT-GTCCCGAA-3′. After construction, the DNA sequences of the plasmids were confirmed by DNA sequence analysis.

Cell Culture and Transfection—The mouse neuroblastoma cell line Neuro2a, the human neuroblastoma cell line SH-SY5Y, and the monkey kidney-derived cell line COS-7 were maintained in Dulbecco's modified Eagle's medium (Sigma) supplemented with 10% fetal calf serum (JRH Biosciences, Lenexa, KS). Transient expression of each vector in Neuro2a and COS-7 cells was performed using the FuGENE 6 transfection reagent (Roche Applied Science). For experiments with differentiated Neuro2a cells, the medium was changed to differentiation medium (Dulbecco's modified Eagle's medium supplemented with 1% fetal calf serum and 20 μM retinoic acid) 24 h after transfection. Approximately 90% of cells in dishes (wells) were transfected in our experimental conditions (data not shown), and there was no notable differences in the transfection efficiency among the wells (supplemental Fig. S1).

Treatment of Cells with Epoxomicin, 3-Methyladenine, Cycloheximide, Rapamycin, or NH_4Cl—Cells grown in 12- or 6-well plates to 50–80% confluence were transfected with expression plasmids containing wild-type, A4V, G85R, or G93A mutant SOD1. 24 h after transfection, cells were incubated with epoxomicin (10 nM, 1 μM, 5 μM, or 10 μM; Sigma), 3-methyladenine (3-MA) (10, 20, or 30 mM; Sigma), rapamycin (100 or 200 nM; Sigma), 20 mM NH_4Cl, and/or carrier (Me_2SO or water) as a control. In some experiments, 10 μg/ml cycloheximide (Sigma) was added to the cells to avoid the confounding effects of ongoing protein synthesis. Epoxomicin, cycloheximide, and rapamycin were dissolved in Me_2SO, NH_4Cl in water. 3-MA was freshly dissolved in culture medium 30 min before use.

Cell Fractionation—For preparation of nonionic detergent-soluble and -insoluble fractions, adherent cells were harvested and lysed on ice for 15 min in 1% Triton X-100 lysis buffer containing 50 mM Tris-HCl, pH 7.5, 150 mM NaCl, 5 mM EDTA, 1% Triton X-100, and protease inhibitors (Complete, EDTA-free; Roche Applied Science). Lysates were centrifuged at 20,000 × *g* for 10 min at 4 °C, and the supernatants were pooled and designated as the detergent-soluble fractions. After the pellets were washed with 1% Triton X-100 lysis buffer, they were solubilized with SDS buffer (50 mM Tris-HCl, pH 7.5, 150 mM NaCl, 5 mM EDTA, 3% SDS, 1% Triton X-100, and protease inhibitors) and sonicated. The resulting solution was used as the detergent-insoluble fraction. For preparation of total cell lysates containing both detergent-soluble and -insoluble fractions, cells were lysed in SDS buffer and sonicated. Protein concentrations were determined with the protein assay kit (Bio-Rad) or the DC protein assay kit (Bio-Rad).

Western Blot Analysis—Western blotting was performed using standard procedures as described previously (20). The primary antibodies used were as follows: anti-SOD1 rabbit polyclonal antibody (1:4000; Stressgen Bioreagents, Victoria, Canada), anti-α-tubulin mouse monoclonal antibody (1:4000; Sigma), anti-β-actin mouse monoclonal antibody (1:5000; Sigma), anti-HA mouse monoclonal antibody (1:4000; Sigma), anti-Beclin 1 mouse monoclonal antibody (1:500; BD Transduction Laboratories, San Diego, CA), anti-Apg7/Atg7 rabbit polyclonal antibody (1:500; Rockland, Gilbertsville, PA). After overnight incubation with primary antibodies at 4 °C, each blot was probed with horseradish peroxidase-conjugated anti-rabbit IgG or anti-mouse IgG (1:20,000; Pierce). Immunoreactive signals were visualized with SuperSignal West Dura extended duration substrate (Pierce) or SuperSignal West Femto maximum sensitivity substrate (Pierce) and detected with a chemiluminescence imaging system (FluorChem; Alpha Innotech, San Leandro, CA). The signal intensity was quantified by densitometry using FluorChem software (Alpha Innotech).

Short Interfering RNA (siRNA) Preparation and Transfection—Double-stranded siRNA targeting mouse Beclin 1, mouse Atg7 and EGFP were purchased from RNAi Co., Ltd.

[3] T. Kabuta, Y. Suzuki, and K. Wada, unpublished data.

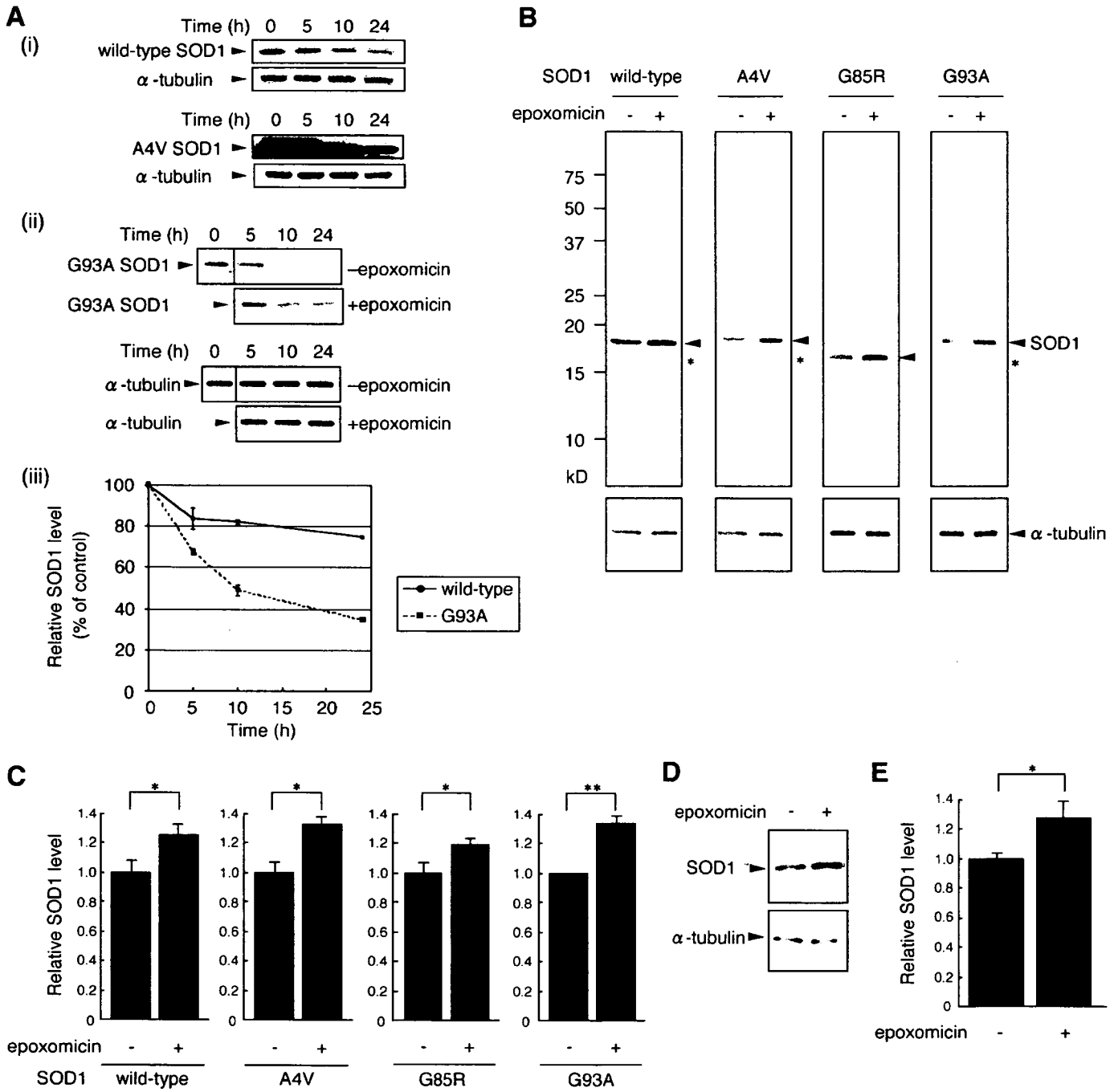

FIGURE 1. **Both mutant and wild-type SOD1 are degraded by the proteasome.** *A, i,* Neuro2a cells were transiently transfected with wild-type or mutant A4V human SOD1. 24 h after transfection, cells were treated with 10 μg/ml cycloheximide for the indicated time and lysed. Total cell lysates were analyzed by immunoblotting using anti-SOD1 or anti-α-tubulin antibody. *ii,* Neuro2a cells transfected with G93A SOD1 were incubated with or without 10 nM epoxomicin in the presence of 10 μg/ml cycloheximide for the indicated time and lysed. Total cell lysates were analyzed by immunoblotting using anti-SOD1 or anti-α-tubulin antibody. *iii,* the relative levels of wild-type or G93A SOD1 (percentage of 0-h control) were quantified by densitometry. Mean values are shown with S.E. ($n = 3$). *B* and *C,* Neuro2a cells were transiently transfected with wild-type or mutant A4V, G85R, or G93A human SOD1. 24 h after transfection, cells were incubated with or without 10 nM epoxomicin in the presence of 10 μg/ml cycloheximide for 24 h. Total cell lysates were analyzed by immunoblotting using anti-SOD1 antibody. The electrophoretic mobility of G85R SOD1 was greater than that of wild-type SOD1. α-Tubulin was used as a loading control. *Asterisks* indicate endogenous mouse SOD1 (*B*). The relative level of wild-type or mutant SOD1 was quantified by densitometry. Mean values are shown with S.E. ($n = 3$). *, $p < 0.05$; **, $p < 0.01$ (*C*). *D* and *E,* human SH-SY5Y cells were incubated with or without 10 nM epoxomicin in the presence of cycloheximide for 24 h. Total cell lysates were analyzed by immunoblotting with anti-SOD1 antibody (*D*). The relative level of human endogenous SOD1 was quantified by densitometry. Data are expressed as the means ± S.E. ($n = 3$). *, $p < 0.05$ (*E*).

(Tokyo, Japan). Sequences targeted by siRNA were selected using siDirect (RNAi Co., Ltd.): mouse Beclin 1 siRNA, sense (5′-GUCUACAGAAAGUGCUAAUAG-3′) and antisense (5′-AUUAGCACUUUCUGUAGACAU-3′); mouse Atg7 siRNA, sense (5′-GAGCGGCGGCUGGUAAGAACA-3′) and antisense (5′-UUCUUACCAGCCGCCGCUCAA-3′); EGFP siRNA, sense (5′-GCCACAACGUCUAUAUCAUGG-3′) and antisense (5′-AUGAUAUAGACGUUGUGGCUG-3′). EGFP siRNA was used as a control. Cells (3×10^5) were cotransfected with 1 μg of DNA and 3 μg of siRNA using Lipofectamine PLUS reagent (Invitrogen).

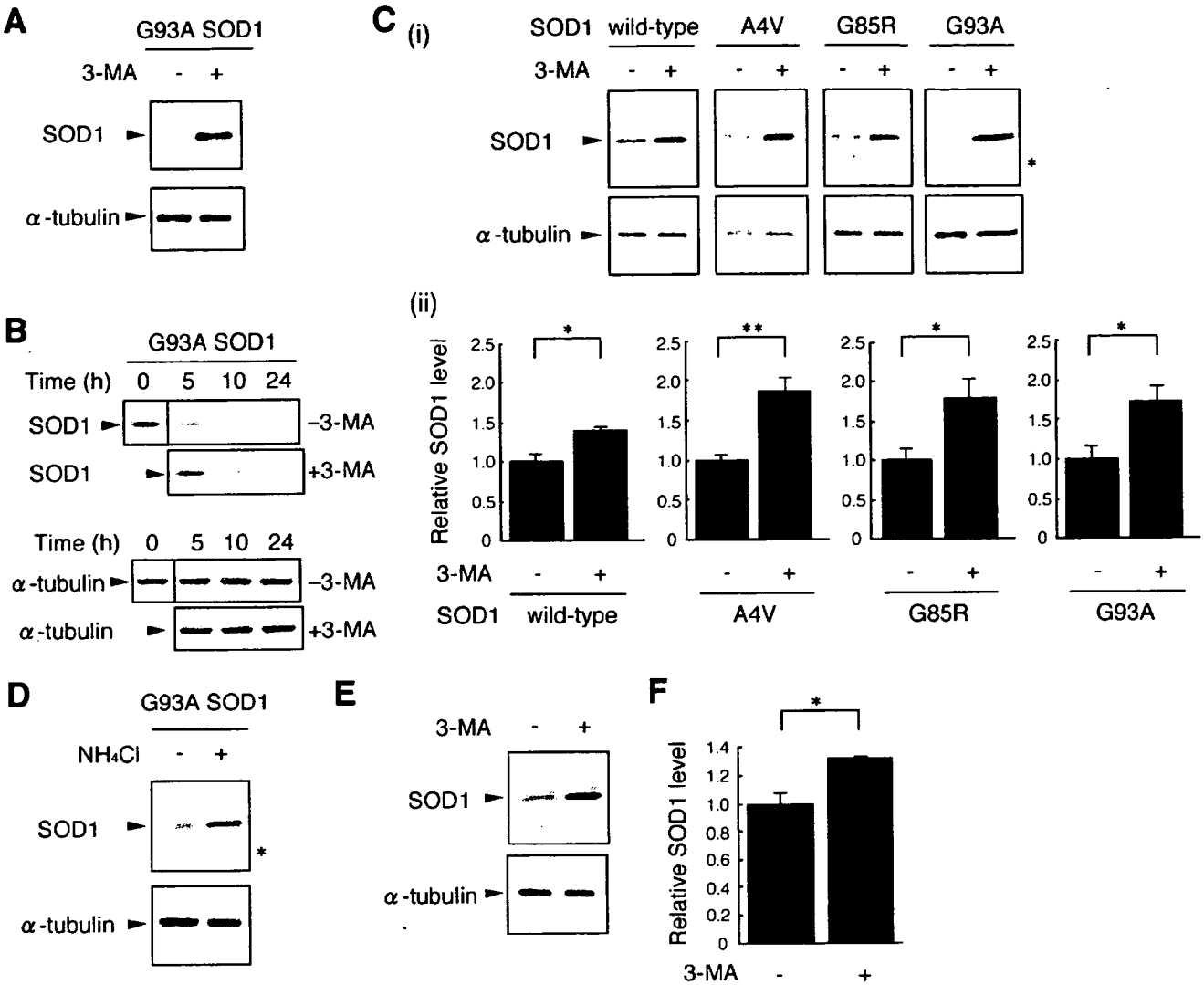

FIGURE 2. **Wild-type and mutant SOD1 are degraded by macroautophagy.** *A*, Neuro2a cells were transiently transfected with the G93A mutant SOD1. 24 h after transfection, cells were incubated with or without 10 mM 3-MA for 24 h. Total cell lysates were analyzed by immunoblotting using anti-SOD1 antibody. α-Tubulin was used as a loading control. *B*, Neuro2a cells transfected with G93A SOD1 were incubated with or without 10 mM 3-MA in the presence of 10 μg/ml cycloheximide for the indicated time and lysed. Total cell lysates were analyzed by immunoblotting using anti-SOD1 or anti-α-tubulin antibody. *C*, Neuro2a cells transfected with wild-type or mutant A4V, G85R, or G93A SOD1 were incubated with or without 10 mM 3-MA in the presence of 10 μg/ml cycloheximide for 24 h. Total cell lysates were analyzed by immunoblotting. An *asterisk* indicates endogenous mouse SOD1 (*i*). The relative level of wild-type or mutant SOD1 was quantified by densitometry. Mean values are shown with S.E. ($n = 3$). *, $p < 0.05$; **, $p < 0.01$ (*ii*). *D*, Neuro2a cells transfected with G93A SOD1 were incubated with or without 20 mM NH_4Cl in the presence of cycloheximide for 24 h. Total cell lysates were analyzed by immunoblotting. An *asterisk* indicates endogenous mouse SOD1. *E* and *F*, SH-SY5Y cells were incubated with or without 10 mM 3-MA in the presence of cycloheximide for 24 h. Total cell lysates were analyzed by immunoblotting (*E*). The relative level of human endogenous SOD1 was quantified by densitometry. Data are expressed as the means ± S.E. ($n = 3$). *, $p < 0.05$ (*F*).

Quantitative Assessment of Cell Viability and Cell Death—One day before transfection, Neuro2a cells were seeded at 5×10^4 cells/well in 24-well plates. 24 h after transfection with 0.4 μg of DNA/well, cells were cultured in differentiation medium with or without 10 mM 3-MA for 24 h. Cell death was assessed by a lactate dehydrogenase release assay using the CytoTox-ONE homogeneous membrane integrity assay (Promega) according to the manufacturer's protocol. The percentage of cytotoxicity (Fig. 7*G*) was calculated according to this protocol. For assessment of cell viability, we used the 3-(4,5-dimethylthiazol-2-yl)-5-(3-carboxymethoxyphenyl)-2-(4-sulfophenyl)-2H-tetrazolium (MTS) assay and the ATP assay with the CellTiter 96 AQueous One Solution cell proliferation assay (Promega) and CellTiter-Glo luminescent cell viability assay (Promega), respectively, according to the manufacturer's protocols. Measurements with a multiple-plate reader were performed after samples were transferred to 96-well assay plates.

Statistical Analysis—For comparison of two groups, the statistical difference was determined by Student's *t* test. For comparison of more than two groups, analysis of variance was used. If the analysis of variance was significant, Dunnett's multiple comparison test was used as a *post hoc* test.

RESULTS

Wild-type and Mutant SOD1 Are Degraded by the Proteasome—To determine whether SOD1 is degraded by the proteasome pathway, we assessed the effect of proteasome inhibitors on SOD1 protein clearance. Peptide aldehydes, such as

MG132 or ALLN, and lactacystin are widely used proteasome inhibitors. However, peptide aldehydes also inhibit cathepsins and calpains, and lactacystin inhibits cathepsin A (21, 22). Because these inhibitors are not proteasome-specific and may interfere with lysosomal function, we used epoxomicin as a selective proteasome inhibitor (23, 24). We observed protein clearance of human SOD1 in Neuro2a cells transfected with mutant or wild-type SOD1 in the presence of the translation inhibitor cycloheximide (Fig. 1*A*, *i* and *ii*). Consistent with previous reports (9, 11), wild-type SOD1 exhibited a relatively long half-life (half-life of more than 24 h) compared with mutant SOD1 (~10 h; G93A) (Fig. 1*A*, *iii*). The degradation of wild-type and mutant SOD1 was suppressed by epoxomicin treatment (Fig. 1, *B* and *C*) (~14-h increase in half-life; G93A; Fig. 1*A*, *ii*). Our finding that mutant SOD1 is degraded by the proteasome is in agreement with previous reports (8, 9). To determine whether endogenous human wild-type SOD1 is also degraded by the proteasome, SOD1 clearance was examined using the human neuroblastoma SH-SY5Y cell line. The proteasome inhibitor treatment promoted the accumulation of human SOD1 proteins (Fig. 1, *D* and *E*). These results indicate that endogenous wild-type SOD1 is degraded by the proteasome, also consistent with a previous report (14).

Wild-type and Mutant SOD1 Are Also Degraded by Macroautophagy—To date, there have been no reports of macroautophagy participating in human SOD1 clearance. We therefore investigated whether wild-type or mutant SOD1 was degraded by macroautophagy using 3-MA, an inhibitor of macroautophagy (18, 25, 26), and ammonium chloride, an inhibitor of lysosomal proteolysis (26). We initially confirmed that 3-MA inhibits the formation of autophagosomes in Neuro2a cells using green fluorescent protein-LC3, a marker of autophagosomes (27) (supplemental Fig. S2). Moreover, we also showed that the clearance of α-synuclein, an established substrate for macroautophagy (28), was inhibited by 3-MA or ammonium chloride treatment (supplemental Fig. S3). Treatment of Neuro2a cells with 3-MA promoted the accumulation of G93A mutant SOD1 proteins (Fig. 2*A*). In the presence of cycloheximide, the degradation of wild-type and mutant SOD1 was suppressed by treatment with 3-MA (Fig. 2, *B* and *C*) (a more than 14-h increase in half-life; G93A, Fig. 2*B*), indicating that wild-type and mutant SOD1 are degraded by macroautophagy in these cells and that the accumulation of SOD1 proteins by 3-MA is not due to increased protein synthesis. These results, together with Fig. 1, suggest that mutant SOD1 are degraded more rapidly than wild-type SOD1 by macroautophagy (it is estimated that 15–20% of wild-type SOD1 and 25–30% of mutant SOD1 were degraded by macroautophagy during the 24-h incubation). The clearance of mutant G93A SOD1 was also decreased by treatment with ammonium chloride (Fig. 2*D*). As shown in Supplemental Fig. S4 and Fig. 2*D*, the protein level of endogenous mouse SOD1 was increased by 3-MA or ammonium chloride treatment. The result shown in Fig. 2*D* further supports the role of the lysosomes in SOD1 degradation. To test the role of macroautophagy on SOD1 degradation in differentiated neuronal cells or neurons, we also used differentiated Neuro2a cells. In differentiated Neuro2a cells, 3-MA increased both wild-type and mutant SOD1 protein levels in the presence or absence of

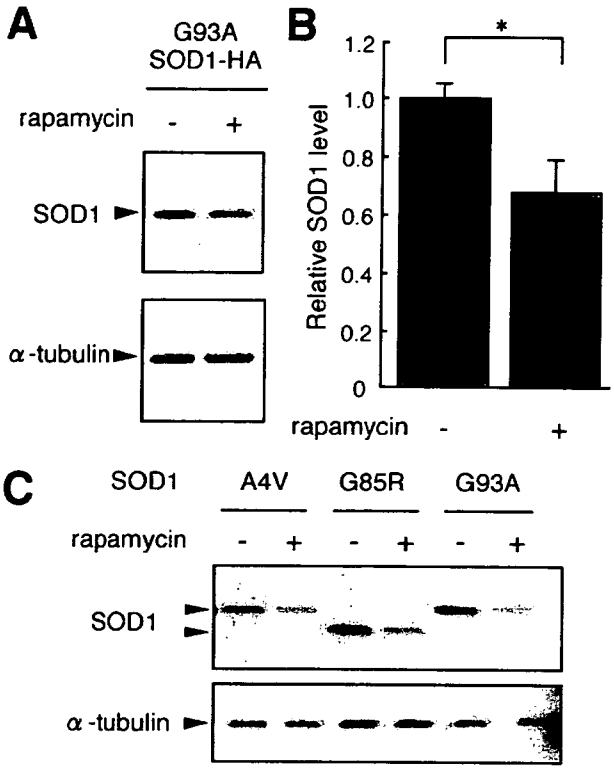

FIGURE 3. **Rapamycin treatment decreases mutant SOD1 protein levels.** *A* and *B*, Neuro2a cells were transiently transfected with HA-tagged G93A SOD1. 24 h after transfection, cells were incubated with or without 100 nM rapamycin for 24 h. Total cell lysates were analyzed by immunoblotting using anti-SOD1 antibody. α-Tubulin was used as a loading control (*A*). The relative level of mutant G93A SOD1 was quantified by densitometry. Data are presented as the means ± S.E. ($n = 3$). *, $p < 0.05$ (*B*). *C*, Neuro2a cells transfected with mutant A4V, G85R, or G93A SOD1 were cultured in differentiation medium with or without 200 nM rapamycin for 24 h. Total cell lysates were analyzed by immunoblotting.

cycloheximide (data not shown). To determine whether endogenous human SOD1 is degraded by macroautophagy, the clearance of endogenous SOD1 was examined in SH-SY5Y cells. As shown in Fig. 2, *E* and *F*, the degradation of endogenous SOD1 proteins was inhibited by 3-MA.

For further confirmation of the clearance of SOD1 by macroautophagy, we used rapamycin to induce macroautophagy (29, 30), and gene silencing with siRNA to inhibit macroautophagy. Treating Neuro2a cells with rapamycin decreased HA-tagged G93A SOD1 levels (Fig. 3, *A* and *B*). In differentiated Neuro2a cells, SOD1 protein levels were also decreased by rapamycin (Fig. 3*C*). Beclin 1 is a component of a class III phosphatidylinositol 3-kinase complex that is crucial for macroautophagy (31). Silencing of the Beclin 1 gene by siRNA inhibits the generation of autophagosomes, thus preventing macroautophagy (32). Atg7 protein is also essential for macroautophagy (17). We initially confirmed that Beclin 1 or Atg7 expression was knocked down by Beclin 1 or Atg7 siRNA, respectively (Fig. 4, *A* and *B*). We also showed that α-synuclein level was increased by Beclin 1 or Atg7 siRNA (supplemental Fig. S3). We observed inhibited degradation of wild-type and mutant SOD1 in cells with Beclin 1 siRNA (Fig. 4, *A* and *C*) or Atg7 siRNA (Fig. 4, *B* and *D*) compared with cells with control siRNA (~14 h increase in half-life; G93A; Fig. 4*E*). The results shown in Figs. 2–4 demonstrate that wild-type and mutant SOD1 are also

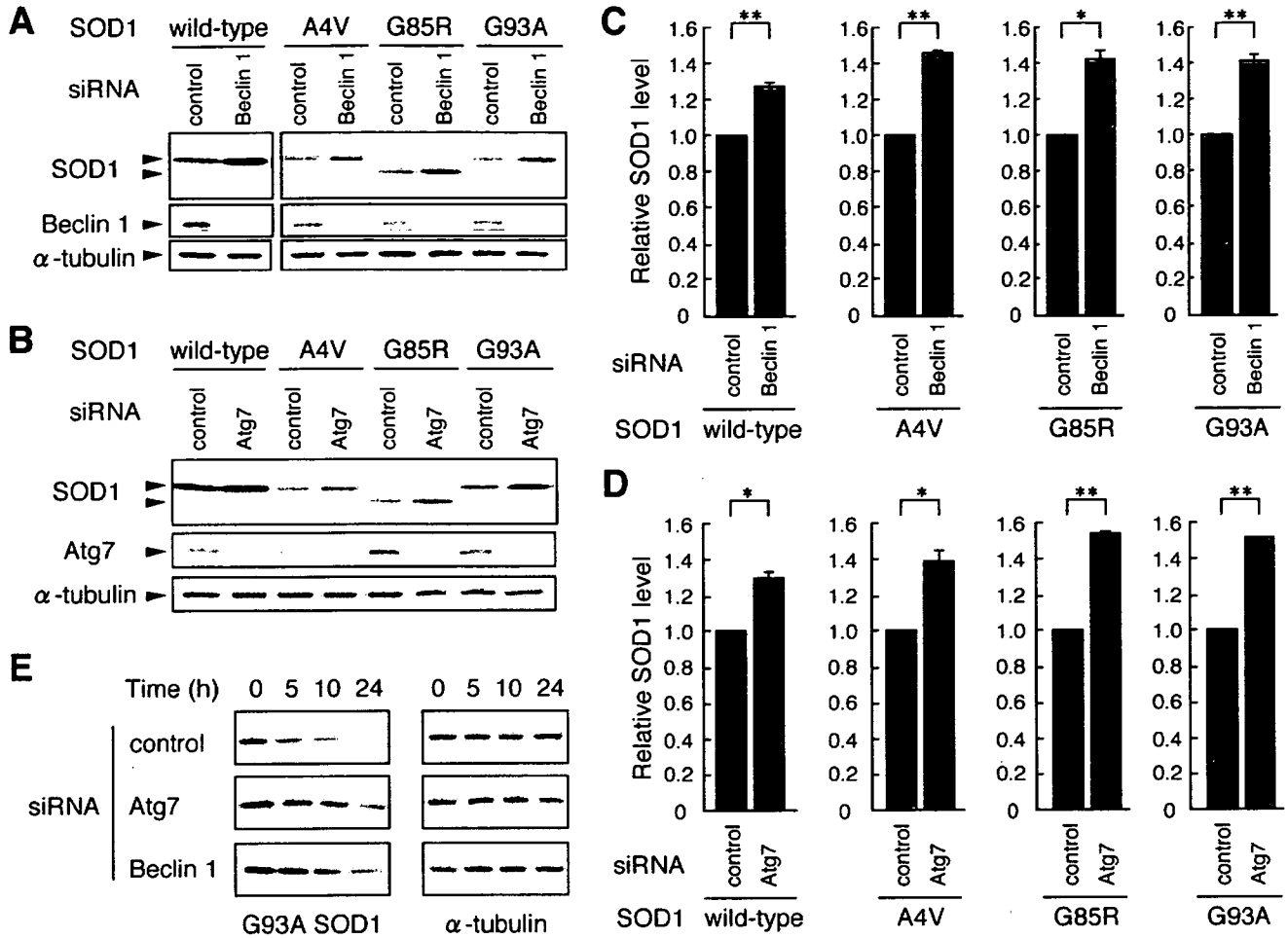

FIGURE 4. **Silencing of macroautophagy genes promote the accumulation of SOD1 proteins.** *A* and *C*, Neuro2a cells were cotransfected with SOD1 (wild-type, A4V, G85R, or G93A) and siRNA (Beclin 1 siRNA or control EGFP siRNA). 24 h after transfection, total cell lysates were prepared and analyzed by immunoblotting using anti-SOD1 or anti-Beclin 1 antibody. α-Tubulin was used as a control (*A*). Levels of SOD1 were quantified by densitometry, and the levels are expressed as -fold level of SOD1 in cells with Beclin 1 siRNA over cells with control siRNA. Data are presented as the means ± S.E. ($n = 3$). *, $p < 0.05$; **, $p < 0.01$ (*C*). *B* and *D*, Neuro2a cells were cotransfected with SOD1 (wild-type, A4V, G85R, or G93A) and siRNA (Atg7 siRNA or control siRNA). 24 h after transfection, total cell lysates were prepared and analyzed by immunoblotting using anti-SOD1, anti-Atg7, or anti-α-tubulin antibody (*B*). Levels of SOD1 were quantified by densitometry, and the levels are expressed as -fold level of SOD1 in cells with Atg7 siRNA over cells with control siRNA. Data are presented as the means ± S.E. ($n = 3$). *, $p < 0.05$; **, $p < 0.01$ (*D*). *E*, Neuro2a cells cotransfected with G93A SOD1 and siRNA (control, Atg7, or Beclin 1 siRNA) were treated with 10 μg/ml cycloheximide for the indicated time and lysed. Total cell lysates were analyzed by immunoblotting using anti-SOD1 or anti-α-tubulin antibody.

degraded by macroautophagy in neuronal cells. In the nonneuronal COS-7 cells, ammonium chloride or 3-MA treatment stimulated the accumulation of HA-tagged wild-type SOD1 and G93A SOD1 (Fig. 5*A*) or mutant G93A SOD1 (Fig. 5*B*), respectively. Treatment of the cells with epoxomicin also increased wild-type and mutant SOD1 levels (Fig. 5*C* and supplemental Fig. S5). These results indicate that wild-type and mutant SOD1 are degraded by both macroautophagy and the proteasome in COS-7 cells. The results shown in Figs. 3*A* and 5*A* indicate that not only SOD1 without a tag but also HA-tagged SOD1 is degraded by macroautophagy.

The Contributions of the Proteasome Pathway and Macroautophagy to Mutant SOD1 Degradation Are Comparable—We then assessed the relative contributions of proteasomal degradation and macroautophagy to the clearance of mutant SOD1. As shown in Fig. 6*A*, 10 mM 3-MA entirely suppresses the (3-MA-sensitive) macroautophagy-mediated degradation of mutant SOD1. 1 μM epoxomicin also entirely suppresses the (epoxomicin-sensitive) proteasome-mediated degradation of mutant SOD1 (Fig. 6*B* and supplemental Fig. S6). Therefore, we compared mutant G93A SOD1 levels in 1 μM epoxomicin-treated cells with that of 10 mM 3-MA-treated cells. The SOD1 protein level in 3-MA-treated cells was comparable with that of epoxomicin-treated cells (Fig. 6, *C–F*). An increased accumulation of mutant SOD1 was detected in cells cotreated with both inhibitors compared with that of 3-MA-treated cells or epoxomicin-treated cells (Fig. 6, *E* and *F*). These data further support the idea that mutant SOD1 proteins are degraded by both macroautophagy and the proteasome and indicate that, in these cells, the contribution of macroautophagy to mutant SOD1 clearance is approximately equal to that of the proteasome pathway.

Macroautophagy Reduces the Toxicity of Mutant SOD1—Previous studies have shown that mutant SOD1-expressing cells are more susceptible to cell death induced by proteasome inhibition (33). We examined whether inhibiting the macroautophagy-mediated degradation of mutant SOD1 could also induce cell death in Neuro2a cells using three different assays.

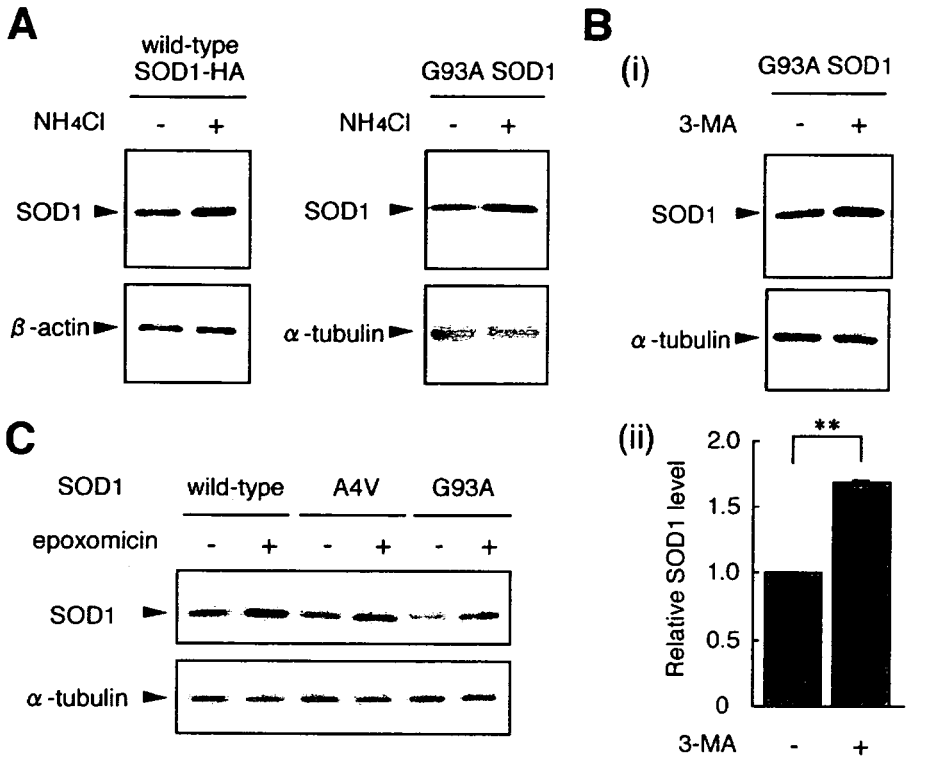

FIGURE 5. **Mutant and wild-type SOD1 are degraded by both macroautophagy and the proteasome in COS-7 cells.** *A*, COS-7 cells were transiently transfected with HA-tagged human wild-type SOD1 or G93A SOD1. 24 h after transfection, cells were incubated with or without 20 mM NH_4Cl for 24 h. Total cell lysates were analyzed by immunoblotting using anti-HA antibody or anti-SOD1 antibody. β-Actin and α-tubulin were used as loading controls. *B*, COS-7 cells transfected with G93A mutant SOD1 were incubated with or without 10 mM 3-MA in the presence of cycloheximide for 24 h. Total cell lysates were analyzed by immunoblotting using anti-SOD1 antibody (*i*). Levels of SOD1 were quantified by densitometry, and the levels are expressed as -fold level of SOD1 in cells with 3-MA over control. Data are presented as the means ± S.E. ($n = 3$). **, $p < 0.01$ (*ii*). *C*, COS-7 cells were transfected with wild-type or mutant A4V or G93A SOD1. 24 h after transfection, cells were incubated with or without 10 nM epoxomicin for 24 h. Total cell lysates were analyzed by immunoblotting.

For assessment of cell viability, we used the MTS assay and ATP assay, and for assessment of cell death, we used the lactate dehydrogenase release assay. In untreated differentiated Neuro2a cells, there was no statistically significant difference in cell viability or cell death among control cells, wild-type SOD1-expressing cells, and mutant SOD1-expressing cells (Fig. 7, *A–C*). However, when cells were treated with 3-MA, mutant SOD1-expressing cells showed significantly increased cell death and significantly decreased cell viability compared with control cells or wild-type SOD1-expressing cells (Fig. 7, *D–F*). When compared with cell death of 3-MA-untreated cells, cell death of 3-MA-treated cells was increased in mutant SOD1-expressed cells but not in cells with wild-type SOD1 (Fig. 7*G*). From these results, we conclude that macroautophagy reduces mutant SOD1-mediated toxicity in this cell model.

Inhibition of Macroautophagy Leads to Accumulation of both Detergent-soluble and Detergent-insoluble Mutant SOD1—Detergent-insoluble SOD1 proteins, aggregates, or inclusion bodies have been found in motor neurons in fALS patients (34), mouse models of fALS (35), and the cells transfected with mutant SOD1 (9, 36), although it is not clear whether these insoluble SOD1 proteins and aggregates are toxic because of conflicting results on the correlation between aggregate formation and cell death (36, 37). We investigated the effect of macroautophagy inhibition on the clearance of nonionic detergent-soluble and -insoluble SOD1. The nonionic detergent-soluble and -insoluble fractions were subjected to SDS-PAGE following Western blotting. In agreement with a previous report (9), mutant SOD1 proteins exhibited increased nonionic detergent insolubility compared with wild-type SOD1 (Fig. 8*B*). The increased level of wild-type SOD1 compared with mutant in the detergent-soluble fraction (Fig. 8*A*) is probably due to the rapid turnover of mutant SOD1. Incubation with 3-MA increased monomer SOD1 levels in the detergent-soluble (Fig. 8*A*) and -insoluble fractions (Fig. 8*B*), suggesting that both detergent-soluble and -insoluble SOD1 are degraded by macroautophagy. Consistent with a previous report (9), we found SDS-resistant dimers and high molecular weight aggregates of mutant SOD1 in the detergent-insoluble fraction (Fig. 8*C*). These dimers and aggregates of mutant SOD1 were increased by 3-MA treatment (Fig. 8*C*), suggesting that insoluble aggregates of mutant SOD1 are also cleared by macroautophagy. The results from Figs. 7 and 8 indicate that the accumulation of toxic mutant SOD1 proteins by macroautophagy inhibition leads to greater cell death.

DISCUSSION

Using inhibitors of macroautophagy and proteasomal degradation, we have shown that both wild-type and mutant SOD1 proteins are degraded by both pathways. Accumulating evidence has shown that mutant SOD1 is degraded by the ubiquitin-proteasome pathway (8, 9, 19). However, most of these studies have used lactacystin or a peptide aldehyde, both of which are not proteasome-specific inhibitors. Our data on the effect of the selective proteasome inhibitor epoxomicin also indicate that mutant SOD1 is degraded by the proteasome. Because wild-type SOD1 is not ubiquitinated by the ubiquitin ligases (10, 11), it has been proposed that wild-type SOD1 is not a substrate of the proteasome. However, a recent report has suggested that wild-type SOD1 can be degraded by the 20 S proteasome without ubiquitination (14). Moreover, we show here that epoxomicin treatment increases both overexpressed and endogenous wild-type SOD1 levels. Our data together with the previous reports support the idea that wild-type SOD1 is degraded by the 20 S proteasome in mammalian cells.

In this study, we demonstrated for the first time that macro-

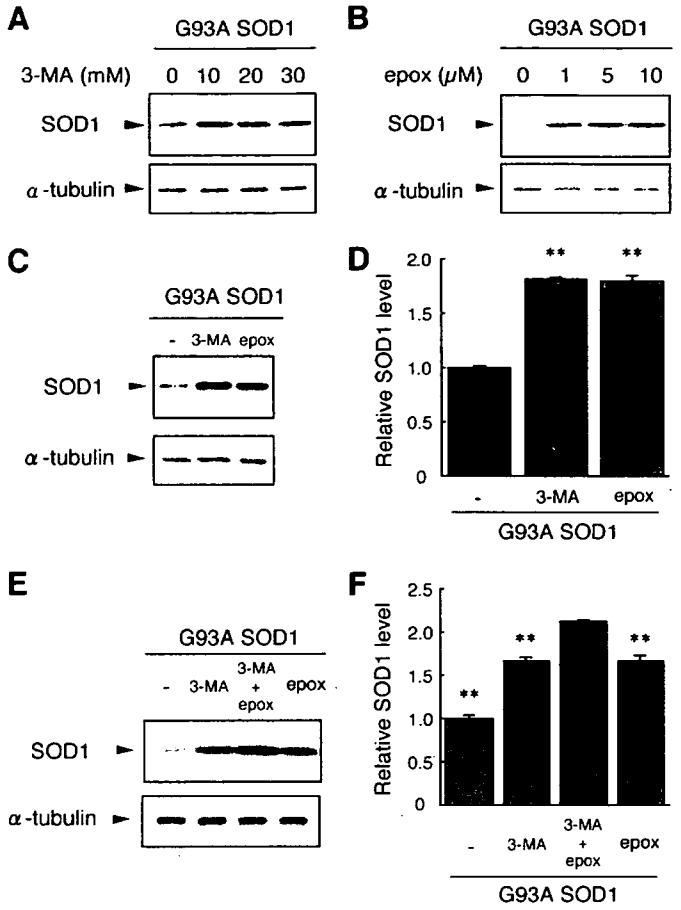

FIGURE 6. **The contribution of macroautophagy to SOD1 clearance is comparable with that of the proteasome.** *A*, Neuro2a cells transfected with mutant G93A SOD1 were incubated with or without 10, 20, or 30 mM 3-MA for 24 h. Total cell lysates were analyzed by immunoblotting. *B*, Neuro2a cells transfected with mutant G93A SOD1 were incubated with or without 1, 5, or 10 μM epoxomicin (*epox*) for 24 h. Total cell lysates were analyzed by immunoblotting. *C* and *D*, Neuro2a cells transfected with mutant G93A SOD1 were incubated with or without 10 mM 3-MA or 1 μM epoxomicin for 24 h. Total cell lysates were analyzed by immunoblotting (*C*). The relative level of mutant G93A SOD1 was quantified by densitometry. Data are presented as the means ± S.E. ($n = 3$). **, $p < 0.01$ in comparison with control (analysis of variance with Dunnett's multiple comparison test). (*D*). *E* and *F*, COS-7 cells transfected with mutant G93A SOD1 were incubated with or without 10 mM 3-MA, 1 μM epoxomicin, or both inhibitors (10 mM 3-MA and 1 μM epoxomicin) in the presence of cycloheximide for 24 h. Total cell lysates were analyzed by immunoblotting (*E*). The relative level of mutant G93A SOD1 was quantified by densitometry. Data are presented as the means ± S.E. ($n = 3$). **, $p <$ 0.01 in comparison with 3-MA + epoxomicin (analysis of variance with Dunnett's multiple comparison test) (*F*).

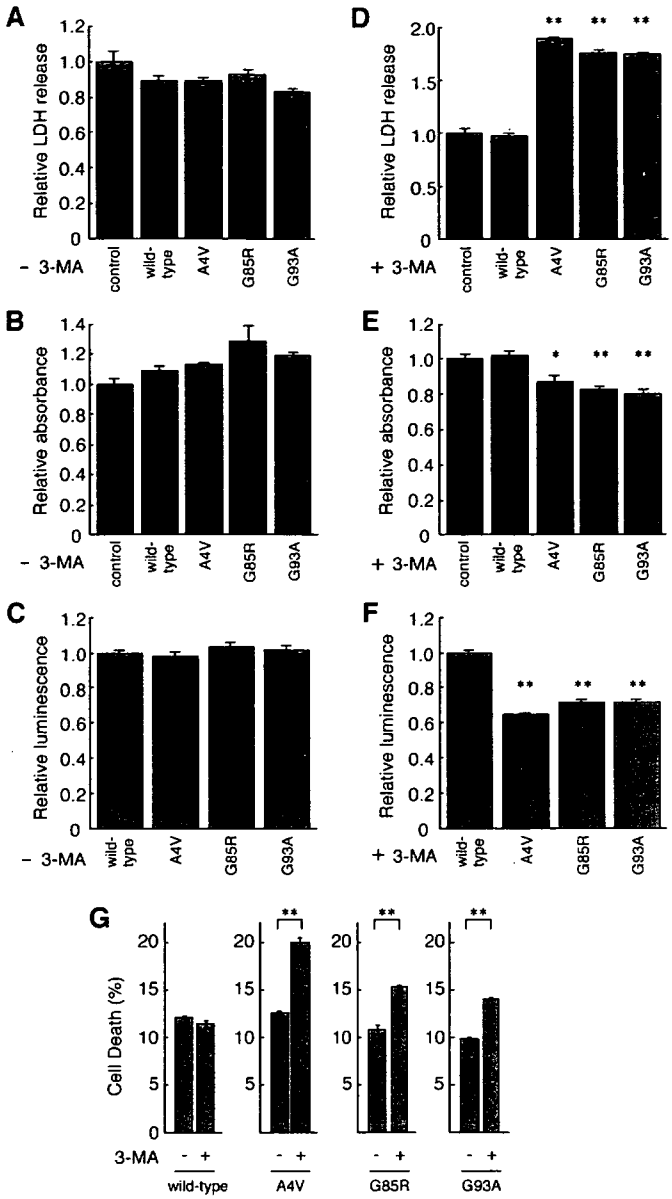

FIGURE 7. **Macroautophagy inhibition causes mutant SOD1-mediated cell death.** *A–G*, Neuro2a cells were transiently transfected with control empty vector (*A*, *B*, *D*, and *E*) or human SOD1 (wild type, A4V, G85R, or G93A). 24 h after transfection, cells were incubated in differentiation medium with (*D–G*) or without (*A–C* and *G*) 10 mM 3-MA for 24 h, and the lactate dehydrogenase release assay (*A*, *D*, and *G*), MTS assay (*B* and *E*), or ATP assay (*C* and *F*) were performed. The percentage of nonviable cells in each sample was calculated from the lactate dehydrogenase release assay (*G*). The experiment in *G* was performed independently of *A* and *D*. Data are expressed as the means ± S.E. ($n = 4$ in *A*, *C*, *D*, *F*, and *G*; $n = 3$ in *B* and *E*). *, $p < 0.05$; **, $p < 0.01$ in comparison with control (*A*, *B*, *D*, and *E*) or with wild-type SOD1 (*C* and *F*) (analysis of variance with Dunnett's multiple comparison test). **, $p < 0.01$ (*G*; *t* test).

autophagy is another pathway for degradation of wild-type and mutant SOD1. Our findings are consistent with a previous report that rat wild-type SOD1 is present in autophagosomes and lysosomes in rat hepatocytes (although they did not examine whether rat SOD1 was degraded by macroautophagy in those cells) (38). We propose that the contribution of macroautophagy to mutant SOD1 degradation is comparable with that of the proteasome pathway in the cell types we tested. Recent studies have demonstrated that transgenic mice with neuron-specific expression of mutant SOD1 do not exhibit an ALS-like phenotype (39, 40) and that neurodegeneration is delayed when motor neurons expressing mutant SOD1 are surrounded by healthy nonneuronal wild-type cells (41). In addition, Urushitani *et al.* (42) have shown that chromogranins promote secretion of mutant SOD1 from cells expressing the mutant protein, and they proposed that secreted mutant SOD1 can be toxic to neighboring cells. These studies strongly suggest that the expression of mutant SOD1 in nonneuronal cells may be involved in mutant SOD1-mediated neurotoxicity. In nonneuronal COS-7 cells, mutant SOD1 is also degraded by both the proteasome and macroautophagy (Fig. 5). Thus, not only the proteasome but also macroautophagy may play an important

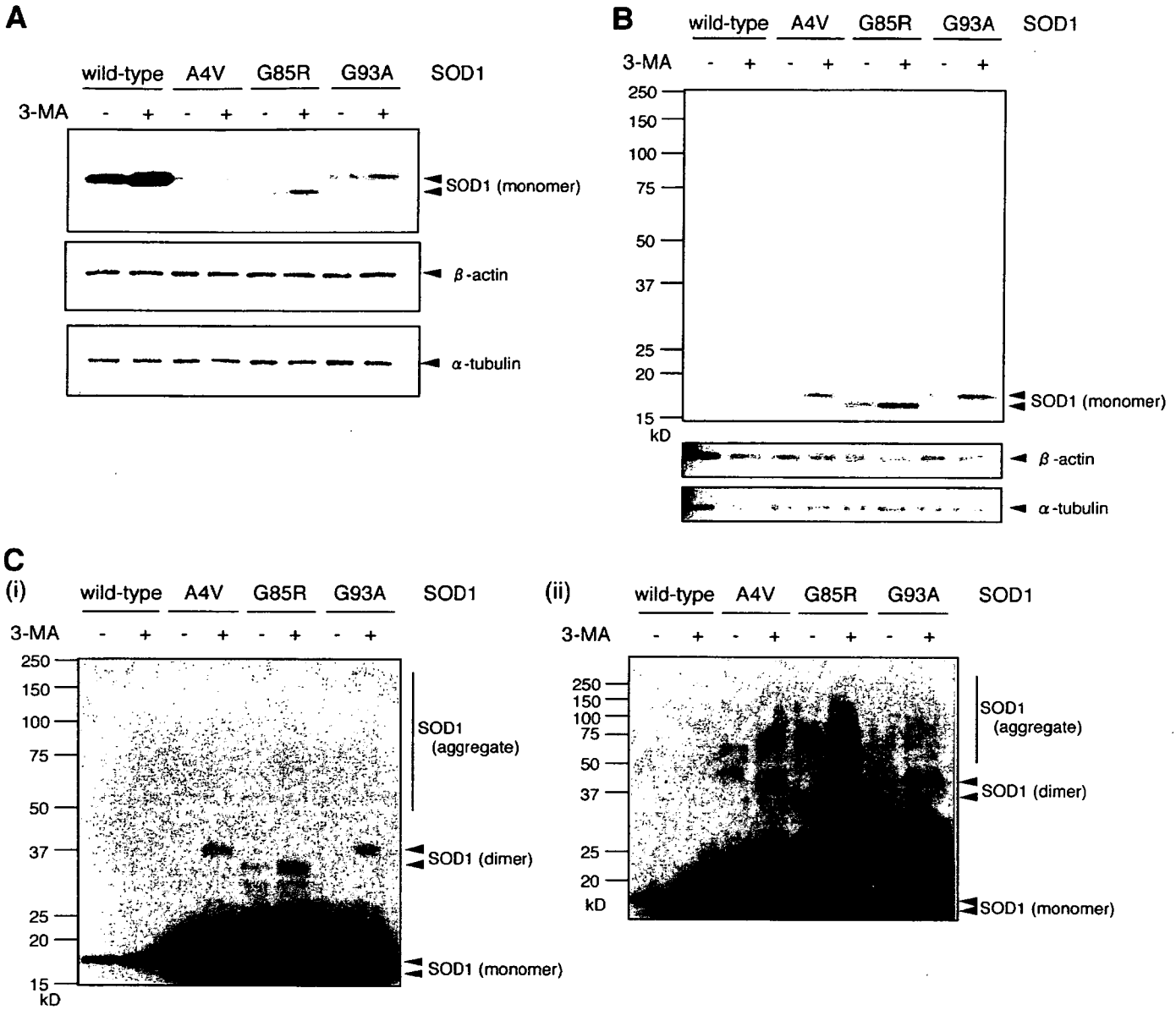

FIGURE 8. **Inhibition of macroautophagy causes accumulation of both detergent-soluble and -insoluble mutant SOD1.** *A–C*, Neuro2a cells were transiently transfected with human wild-type or mutant A4V, G85R, or G93A SOD1. 24 h after transfection, cells were cultured in differentiation medium with or without 10 mM 3-MA for 24 h. Triton X-100-soluble (*A*) and -insoluble (*B* and *C*) fractions were prepared and analyzed by immunoblotting using anti-SOD1 antibody. β-Actin and α-tubulin were used as loading controls. *C* (*i*), a longer exposure of *B*. C (*i* and *ii*), two different sets of experiments with longer exposure.

role in clearance of mutant SOD1 in fALS in nonneuronal cells as well as in neuronal cells.

It has been well established that mutant SOD1-mediated toxicity is caused by a gain of toxic function rather than the loss of SOD1 activity (1, 2). The appearance of mutant SOD1 aggregates in motor neurons in fALS patients and mouse models of fALS (34, 35) has suggested that aggregation has a role in neurotoxicity. However, conflicting results have been reported on the correlation between aggregate formation and cell death. A recent study has shown that the ability of mutant G85R and G93A SOD1 proteins to form aggregates correlates with neuronal cell death using live cell imaging techniques (36). Another report has concluded that aggregate formation of A4V and V148G SOD1 mutants does not correlate with cell death (37). These controversies also exist in other neurodegenerative diseases (43–46). Our current data suggest that macroautophagy degrades toxic species of mutant SOD1 and that the accumulation of mutant SOD1 proteins leads to greater cell death. However, whether the toxic SOD1 species are monomers, oligomers, or aggregates cannot be determined from our study, because a variety of mutant SOD1 species, including detergent-soluble SOD1 monomers and detergent-insoluble monomers, dimers, and aggregates, were accumulated by macroautophagy inhibition (Fig. 8).

Our data show that macroautophagy reduces mutant SOD1-mediated toxicity and that induction of macroautophagy decreases mutant SOD1 protein levels. Niwa *et al.* (10) have shown that the ubiquitin ligase Dorfin ubiquitinates mutant SOD1 and prevents the neurotoxicity of mutant SOD1. Taken together, these data imply that macroautophagy inducers, acti-

vators of the ubiquitin-proteasome pathway, or a combination of the two have therapeutic potential for fALS. In conclusion, our results demonstrate that mutant SOD1 is degraded by at least two pathways, macroautophagy and the proteasome pathway, and that the clearance of mutant SOD1 by macroautophagy reduces its cell toxicity. These findings may provide insight into the molecular mechanisms of the pathogenesis of fALS.

Acknowledgments—We thank Dr. Ryosuke Takahashi (Kyoto University) and Dr. Makoto Urushitani (Laval University) for the gift of pcDNA3-hSOD1 (wild-type and mutant A4V, G85R, and G93A) plasmids, and Naoki Takagaki for the support in English.

REFERENCES

1. Bruijn, L. I., Miller, T. M., and Cleveland, D. W. (2004) *Annu. Rev. Neurosci.* **27,** 723–749
2. Cleveland, D. W., and Rothstein, J. D. (2001) *Nat. Rev. Neurosci.* **2,** 806–819
3. Rosen, D. R., Siddique, T., Patterson, D., Figlewicz, D. A., Sapp, P., Hentati, A., Donaldson, D., Goto, J., O'Regan, J. P., Deng, H. X., Rahmani, Z., Krizus, A., McKenna-Yasek, D., Cayabyab, A., Gaston, S. M., Berger, R., Tanzi, R. E., Halperin, J. J., Herzfeldt, B., Van den Bergh, R., Hung, W. Y., Bird, T., Deng, G., Mulder, D. W., Smyth, C., Laing, N. G., Soriano, E., Pericak-Vance, M. A., Haines, J., Rouleau, G. A., Gusella, J. S., Horvitz, H. R., and Brown, R. H., Jr. (1993) *Nature* **362,** 59–62
4. Gurney, M. E., Pu, H., Chiu, A. Y., Dal Canto, M. C., Polchow, C. Y., Alexander, D. D., Caliendo, J., Hentati, A., Kwon, Y. W., Deng, H. X., Chen, W., Zhai, P., Sufit, R. L., and Siddique, T. (1994) *Science* **264,** 1772–1775
5. Reaume, A. G., Elliott, J. L., Hoffman, E. K., Kowall, N. W., Ferrante, R. J., Siwek, D. F., Wilcox, H. M., Flood, D. G., Beal, M. F., Brown, R. H., Jr., Scott, R. W., and Snider, W. D. (1996) *Nat. Genet.* **13,** 43–47
6. Goldberg, A. L. (2003) *Nature* **426,** 895–899
7. Cuervo, A. M. (2004) *Trends Cell Biol.* **14,** 70–77
8. Hoffman, E. K., Wilcox, H. M., Scott, R. W., and Siman, R. (1996) *J. Neurol. Sci.* **139,** 15–20
9. Johnston, J. A., Dalton, M. J., Gurney, M. E., and Kopito, R. R. (2000) *Proc. Natl. Acad. Sci. U. S. A.* **97,** 12571–12576
10. Niwa, J., Ishigaki, S., Hishikawa, N., Yamamoto, M., Doyu, M., Murata, S., Tanaka, K., Taniguchi, N., and Sobue, G. (2002) *J. Biol. Chem.* **277,** 36793–36798
11. Miyazaki, K., Fujita, T., Ozaki, T., Kato, C., Kurose, Y., Sakamoto, M., Kato, S., Goto, T., Itoyama, Y., Aoki, M., and Nakagawara, A. (2004) *J. Biol. Chem.* **279,** 11327–11335
12. Shringarpure, R., Grune, T., Mehlhase, J., and Davies, K. J. (2003) *J. Biol. Chem.* **278,** 311–318
13. Asher, G., Tsvetkov, P., Kahana, C., and Shaul, Y. (2005) *Genes Dev.* **19,** 316–321
14. Di Noto, L., Whitson, L. J., Cao, X., Hart, P. J., and Levine, R. L. (2005) *J. Biol. Chem.* **280,** 39907–39913
15. Komatsu, M., Waguri, S., Chiba, T., Murata, S., Iwata, J., Tanida, I., Ueno, T., Koike, M., Uchiyama, Y., Kominami, E., and Tanaka, K. (2006) *Nature* **441,** 880–884
16. Hara, T., Nakamura, K., Matsui, M., Yamamoto, A., Nakahara, Y., Suzuki-Migishima, R., Yokoyama, M., Mishima, K., Saito, I., Okano, H., and Mizushima, N. (2006) *Nature* **441,** 885–889
17. Komatsu, M., Waguri, S., Ueno, T., Iwata, J., Murata, S., Tanida, I., Ezaki, J., Mizushima, N., Ohsumi, Y., Uchiyama, Y., Kominami, E., Tanaka, K., and Chiba, T. (2005) *J. Cell Biol.* **169,** 425–434
18. Ravikumar, B., Duden, R., and Rubinsztein, D. C. (2002) *Hum. Mol. Genet.* **11,** 1107–1117
19. Urushitani, M., Kurisu, J., Tsukita, K., and Takahashi, R. (2002) *J. Neurochem.* **83,** 1030–1042
20. Kabuta, T., Hakuno, F., Asano, T., and Takahashi, S. (2002) *J. Biol. Chem.* **277,** 6846–6851
21. Lee, D. H., and Goldberg, A. L. (1998) *Trends Cell Biol.* **8,** 397–403
22. Ostrowska, H., Wojcik, C., Wilk, S., Omura, S., Kozlowski, L., Stoklosa, T., Worowski, K., and Radziwon, P. (2000) *Int. J. Biochem. Cell Biol.* **32,** 747–757
23. Meng, L., Mohan, R., Kwok, B. H., Elofsson, M., Sin, N., and Crews, C. M. (1999) *Proc. Natl. Acad. Sci. U. S. A.* **96,** 10403–10408
24. Garcia-Echeverria, C. (2002) *Mini Rev. Med. Chem.* **2,** 247–259
25. Qin, Z. H., Wang, Y., Kegel, K. B., Kazantsev, A., Apostol, B. L., Thompson, L. M., Yoder, J., Aronin, N., and DiFiglia, M. (2003) *Hum. Mol. Genet.* **12,** 3231–3244
26. Cuervo, A. M., Stefanis, L., Fredenburg, R., Lansbury, P. T., and Sulzer, D. (2004) *Science* **305,** 1292–1295
27. Kabeya, Y., Mizushima, N., Ueno, T., Yamamoto, A., Kirisako, T., Noda, T., Kominami, E., Ohsumi, Y., and Yoshimori, T. (2000) *EMBO J.* **19,** 5720–5728
28. Webb, J. L., Ravikumar, B., Atkins, J., Skepper, J. N., and Rubinsztein, D. C. (2003) *J. Biol. Chem.* **278,** 25009–25013
29. Blommaart, E. F., Luiken, J. J., Blommaart, P. J., van Woerkom, G. M., and Meijer, A. J. (1995) *J. Biol. Chem.* **270,** 2320–2326
30. Gutierrez, M. G., Master, S. S., Singh, S. B., Taylor, G. A., Colombo, M. I., and Deretic, V. (2004) *Cell* **119,** 753–766
31. Liang, X. H., Jackson, S., Seaman, M., Brown, K., Kempkes, B., Hibshoosh, H., and Levine, B. (1999) *Nature* **402,** 672–676
32. Shimizu, S., Kanaseki, T., Mizushima, N., Mizuta, T., Arakawa-Kobayashi, S., Thompson, C. B., and Tsujimoto, Y. (2004) *Nat. Cell Biol.* **6,** 1221–1228
33. Aquilano, K., Rotilio, G., and Ciriolo, M. R. (2003) *J. Neurochem.* **85,** 1324–1335
34. Kato, S., Takikawa, M., Nakashima, K., Hirano, A., Cleveland, D. W., Kusaka, H., Shibata, N., Kato, M., Nakano, I., and Ohama, E. (2000) *Amyotroph. Lateral Scler. Other Motor Neuron Disord.* **1,** 163–184
35. Bruijn, L. I., Becher, M. W., Lee, M. K., Anderson, K. L., Jenkins, N. A., Copeland, N. G., Sisodia, S. S., Rothstein, J. D., Borchelt, D. R., Price, D. L., and Cleveland, D. W. (1997) *Neuron* **18,** 327–338
36. Matsumoto, G., Stojanovic, A., Holmberg, C. I., Kim, S., and Morimoto, R. I. (2005) *J. Cell Biol.* **171,** 75–85
37. Lee, J. P., Gerin, C., Bindokas, V. P., Miller, R., Ghadge, G., and Roos, R. P. (2002) *J. Neurochem.* **82,** 1229–1238
38. Rabouille, C., Strous, G. J., Crapo, J. D., Geuze, H. J., and Slot, J. W. (1993) *J. Cell Biol.* **120,** 897–908
39. Pramatarova, A., Laganiere, J., Roussel, J., Brisebois, K., and Rouleau, G. A. (2001) *J. Neurosci.* **21,** 3369–3374
40. Lino, M. M., Schneider, C., and Caroni, P. (2002) *J. Neurosci.* **22,** 4825–4832
41. Clement, A. M., Nguyen, M. D., Roberts, E. A., Garcia, M. L., Boillee, S., Rule, M., McMahon, A. P., Doucette, W., Siwek, D., Ferrante, R. J., Brown, R. H., Jr., Julien, J. P., Goldstein, L. S., and Cleveland, D. W. (2003) *Science* **302,** 113–117
42. Urushitani, M., Sik, A., Sakurai, T., Nukina, N., Takahashi, R., and Julien, J. P. (2006) *Nat. Neurosci.* **9,** 108–118
43. Arrasate, M., Mitra, S., Schweitzer, E. S., Segal, M. R., and Finkbeiner, S. (2004) *Nature* **431,** 805–810
44. Saudou, F., Finkbeiner, S., Devys, D., and Greenberg, M. E. (1998) *Cell* **95,** 55–66
45. Schaffar, G., Breuer, P., Boteva, R., Behrends, C., Tzvetkov, N., Strippel, N., Sakahira, H., Siegers, K., Hayer-Hartl, M., and Hartl, F. U. (2004) *Mol. Cell* **15,** 95–105
46. Nucifora, F. C., Jr., Sasaki, M., Peters, M. F., Huang, H., Cooper, J. K., Yamada, M., Takahashi, H., Tsuji, S., Troncoso, J., Dawson, V. L., Dawson, T. M., and Ross, C. A. (2001) *Science* **291,** 2423–2428

Available online at www.sciencedirect.com

ScienceDirect

Neurochemistry International 50 (2007) 119–129

NEUROCHEMISTRY International

www.elsevier.com/locate/neuint

Dopaminergic neuronal loss in transgenic mice expressing the Parkinson's disease-associated UCH-L1 I93M mutant

Rieko Setsuie [a,b,1], Yu-Lai Wang [a,1], Hideki Mochizuki [c,d], Hitoshi Osaka [a,e], Hideki Hayakawa [c], Nobutsune Ichihara [f], Hang Li [a], Akiko Furuta [a], Yae Sano [a,b], Ying-Jie Sun [a], Jungkee Kwon [a,g], Tomohiro Kabuta [a], Kenji Yoshimi [d], Shunsuke Aoki [a], Yoshikuni Mizuno [c,d], Mami Noda [b], Keiji Wada [a,*]

[a] *Department of Degenerative Neurological Diseases, National Institute of Neuroscience, National Center of Neurology and Psychiatory, Kodaira, Tokyo 187-8502, Japan*

[b] *Laboratory of Pathophysiology, Graduate School of Pharmaceutical Sciences, Kyushu University, Higashi-ku, Fukuoka 812-8582, Japan*

[c] *Department of Neurology, Juntendo University School of Medicine, Bunkyo-ku, Tokyo 113-8421, Japan*

[d] *Research Institute for Diseases of Old Age, Juntendo University School of Medicine, Bunkyo-ku, Tokyo 113-8421, Japan*

[e] *Division of Neurology, Clinical Research Institute, Kanagawa Children's Medical Center, Yokohama 232-8555, Japan*

[f] *Department of Anatomy, School of Veterinary Medicine, Azabu University, Sagamihara 229-8501, Japan*

[g] *College of Veterinary Medicine, Chonbuk National University, 644-14 Duckjin-Ku, Jeonju 561-756, Republic of Korea*

Received 14 March 2006; received in revised form 19 June 2006; accepted 11 July 2006
Available online 11 September 2006

Abstract

The I93M mutation in ubiquitin carboxyl-terminal hydrolase L1 (UCH-L1) was reported in one German family with autosomal dominant Parkinson's disease (PD). The causative role of the mutation has, however, been questioned. We generated transgenic (Tg) mice carrying human *UCHL1* under control of the *PDGF-B* promoter; two independent lines were generated with the I93M mutation (a high- and low-expressing line) and one line with wild-type human UCH-L1. We found a significant reduction in the dopaminergic neurons in the substantia nigra and the dopamine content in the striatum in the high-expressing I93M Tg mice as compared with non-Tg mice at 20 weeks of age. Although these changes were absent in the low-expressing I93M Tg mice. 1-methyl-4-phenyl-1,2,3,6-tetrahydropyridine (MPTP) treatment profoundly reduced dopaminergic neurons in this line as compared with wild-type Tg or non-Tg mice. Abnormal neuropathologies were also observed, such as silver staining-positive argyrophilic grains in the perikarya of degenerating dopaminergic neurons, in I93M Tg mice. The midbrains of I93M Tg mice contained increased amounts of insoluble UCH-L1 as compared with those of non-Tg mice, perhaps resulting in a toxic gain of function. Collectively, our data represent *in vivo* evidence that expression of *UCHL1*^{I93M} leads to the degeneration of dopaminergic neurons.

Keywords: Ubiquitin carboxy-terminal hydrolase L1; Animal model; Parkinson's disease; Dopaminergic neuron

1. Introduction

Parkinson's disease (PD) is the second most common human neurodegenerative disorder after Alzheimer's disease (AD) (Dauer and Przedborski, 2003; Vila and Przedborski, 2004). PD patients exhibit motor dysfunction, including slowed movement (bradykinesia), resting tremor, rigidity, and postural instability (Dauer and Przedborski, 2003). The pathological basis of PD is the progressive loss of dopaminergic neurons in the substantia nigra pars compacta, giving rise to a decrease in dopamine content in the striatum (Dauer and Przedborski, 2003). Although most cases of PD are sporadic, studies of familial PD have provided accumulating evidence for the molecular mechanisms of PD. Thus far, at least six proteins have been identified to cause familial PD: α-synuclein (Chartier-Harlin et al., 2004; Farrer et al., 2004; Ibanez et al., 2004; Kruger et al., 1998; Polymeropoulos et al., 1997; Singleton et al., 2003), UCH-L1 (Leroy et al., 1998), parkin (Kitada et al., 1998), DJ-1 (Bonifati et al., 2003), phosphatase

* Corresponding author. Tel.: +81 42 346 1715; fax: +81 42 346 1745.
E-mail address: wada@ncnp.go.jp (K. Wada).
[1] These authors contributed equally to this work.

0197-0186/$ – see front matter © 2006 Elsevier Ltd. All rights reserved.
doi:10.1016/j.neuint.2006.07.015

and tensin homolog induced kinase-1 (PINK1) (Valente et al., 2004), and leucine-rich repeat kinase-2 (LRRK2) (Paisan-Ruiz et al., 2004; Zimprich et al., 2004). α-Synuclein, UCH-L1 and LRRK2 are linked to the autosomal dominant form of PD, whereas parkin, DJ-1 and PINK1 are linked to the recessive form.

In 1998, UCH-L1 carrying an Ile to Met mutation at amino acid position 93 (I93M) was identified in one German family affected by autosomal dominant familial PD. UCH-L1, also known as PGP9.5, is an abundant protein in neuronal cells, comprising up to about 1–2% of total protein in the brain. Its function as de-ubiquitylating enzyme (Larsen et al., 1998; Wilkinson et al., 1989), ubiquitylating enzyme (Liu et al., 2002), de-neddylating enzyme (Hemelaar et al., 2004), and mono-ubiquitin stabilizer (Osaka et al., 2003) has been reported. *In vitro* analysis using recombinant human UCH-L1 indicated that I93M mutation results in the reduction of hydrolase activity of about 50% (Nishikawa et al., 2003). *Uchl1* gene deletion in mice, however, was reported to causes gracile axonal dystrophy (*gad*), a recessive neurodegenerative disease with distinct phenotype and pathological features from PD (Saigoh et al., 1999). Moreover, extensive analysis failed to find other PD patients with mutations in the *UCHL1* gene (Lincoln et al., 1999; Maraganore et al., 1999) and there was an incomplete penetrance in reported German family (Leroy et al., 1998). Thus, the correlation of I93M mutation and pathogenesis of PD was questioned.

To elucidate the pathological role of UCH-L1^{I93M} expression in the pathogenesis of PD, *in vivo*, we generated transgenic mice expressing human UCH-L1^{I93M}

2. Experimental procedures

2.1. Generation of hUCHL1^{WT} and hUCHL1^{I93M} transgenic mice

We generated transgenes by cloning either the wild-type or I93M mutant human UCH-L1 cDNAs under the control of the human platelet-derived growth factor B chain (*PDGF-B*) promoter (Fig. 1A) (Sasahara et al., 1991). Sequences encoding *UCHL1* were amplified from a human brain cDNA library (Stratagene, La Jolla, CA) by PCR and subcloned into the *Xho*I and *Not*I sites of pCI-neo (Promega, Madison, WI). The I93M substitution was obtained using QuikChange (Stratagene). The 5′ flanking region of the human *PDGF-B* chain gene was isolated from the human genomic DNA and inserted into the *Bgl*II and *Xho*I site of pCI-neo which results in the replacement of promoter from CMV to *PDGF-B*. The plasmid was linearized by digestion with *Hin*dIII and *Aat*II. A 2 μg/ml solution of the linearized plasmid of each transgene was then microinjected into the pronuclei of newly fertilized C57BL/6J mouse eggs. Offspring were screened for the presence of the transgene by PCR of tail DNA using specific primers (forward: PD-UCH-2, 5′-GCACTCTCCCTTCTCCTTTATA-3′; reverse: PD-UCH-5, 5′-CCTGTATGGCCTCATTCTTTTC-3′). Expression of hUCH-L1^{I93M} in a low-expressing mouse line only occurred in male mice. Thus, all experiments were done using male heterozygous transgenic mice. Animal care and handling were in accordance with institutional regulations for animal care and were approved by the Animal Investigation Committee of the National Institute of Neuroscience, National Center of Neurology and Psychiatry, Tokyo, Japan which conforms the National Institute of Health guide for the care and use of Laboratory animals.

2.2. Quantitative RT-PCR analysis

Primers specific for mouse *Uchl1* (forward: mL1-7, 5′-CCTTGGTTTGCAGCTTTAGCA-3′; reverse: mL1-8, 5′-GGGCTGTAGAACGCAAGAAGA-3′) and human *UCHL1* (forward: L1Tg-F2, 5′-TGGCAACTTCTCCTCCTGCA-3′; reverse: L1Tg-R2, 5′-ACAGCACTTTGTTCAGCATC-3′) were designed, and SYBR Green-based real-time quantitative RT-PCR was performed using the ABI PRISM 7700 (Applied Biosystems, Foster City, CA) using total RNA from mouse brain ($n = 3$ for each line) (Aoki et al., 2002). GAPDH was used as an internal control.

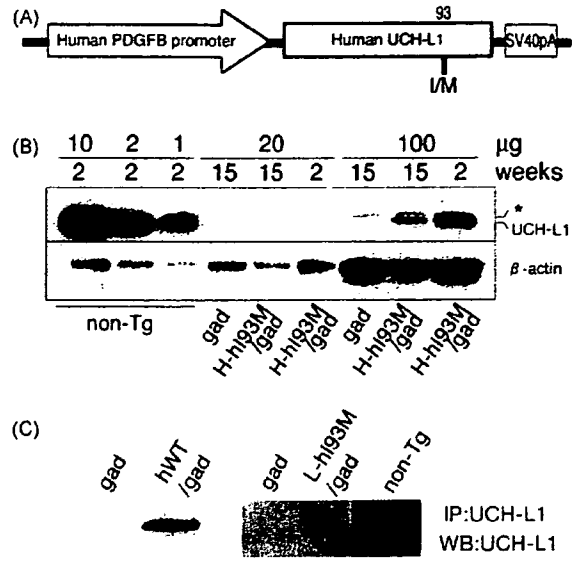

Fig. 1. Generation of transgenic mice expressing hUCH-L1^{WT}and hUCH-L1^{I93M}. (A) UCH-L1^{I93M} was constructed under control of the *PDGF-B* promoter, as depicted. (B) Immunoblotting analysis of endogenous mouse UCH-L1 and transgenic human UCH-L1 expression in mouse midbrain. To detect exogenous human UCH-L1 levels specifically, we generated transgenic mice in the *gad* background (H-hI93M/*gad*), which corresponds to the null mutant of *Uchl1*. Notice that the faint band corresponding to UCH-L1 is detected at 2 weeks of age when 20 μg protein/lane was loaded for the detergent-soluble fraction of midbrain origin in H-hI93M/*gad* mice. When the applied protein was increased to 100 μg/lane, UCH-L1 was easily detected at 2 weeks in H-hI93M/*gad* mice, and UCH-L1 levels markedly decreased by age 15 weeks. Faint bands indicated by the asterisk may correspond to UCH-L3, which cross-reacted with the UCH-L1 antibody when a large amount of protein was loaded per lane. (C) Immunoprecipitation analysis of exogenous human UCH-L1 in hWT/gad (left) and L-hI93M/gad (right) brains. Brain lysates from hWT/gad (left) or L-hI93M/gad (right) were both immunoprecipitated and detected using anti-UCH-L1 antibody. The band corresponding to the UCH-L1 can be found in both hWT/gad and L-hI93M/gad lysates but not in gad lysates indicating the exogenous human UCH-L1 expression.

2.3. Fractionation and immunoblotting and immunoprecipitation

For the immunoblotting of total UCH-L1, the soluble fraction in RIPA (20 mM Tris–HCl, pH 7.5; 0.1% SDS; 1.0% (w/v) Triton X-100; 1.0% sodium deoxycholate) with Complete EDTA-Free Protease Inhibitors (Roche, Basel, Switzerland) was extracted from H-hI93M/*gad* ([high-expressing] *UCH-L1*$^{I93M/-}$, *Uchl1*$^{gad/gad}$), *gad* and non-Tg mouse midbrains. The extracted samples were loaded as indicated in Fig. 1.

For subfractionation, the cortex and hippocampus were removed from the midbrains of a H-hI93M mouse or a non-Tg littermate and bottom half under the aqueduct were used as the substantia nigra fraction. The fractionation method was modified from that of Kahle et al. (2001). Each sample was homogenized with 9 volumes of 5% SDS/TBS lysis buffer (50 mM Tris–HCl (pH 7.5), 150 mM NaCl, 5% SDS) with Complete EDTA-Free Protease Inhibitors using a 23G syringe. After three times of 10 s sonication, samples were ultra-centrifuged in 130,000 × *g* for 1 h, and the supernatant were pooled as 5% SDS fraction. The pellets were washed with 5% SDS/TBS solution once and further homogenized in 8 M urea/5% SDS/TBS lysis buffer

(8 M urea, 5% SDS, 50 mM Tris–HCl (pH 7.5), 150 mM NaCl) with 23G syringe. The resulting supernatant was used as 8 M urea/5% SDS fraction. The protein concentration was assessed by a DC-protein assay kit (Bio-Rad). 1.25 μg of 5% SDS fraction and 0.5 μg of 8 M urea/5% SDS fraction were subjected to SDS-PAGE using 15% gels (Perfect NT Gel; DRC, Tokyo, Japan). Anti-UCH-L1 (1:5000, RA95101; Ultraclone, Isle of Wight, UK) and anti-β-actin (1:5000, clone AC15; Sigma, St. Louis, MO) were used to detect each protein. Signals were detected using a chemiluminescent SuperSignal West Dura Extended Duration Substrate kit or West Femto Maximum Sensitivity Substrate kit (Pierce, Rochford, IL) and analyzed with a Chemilmager (Alpha Innotech, San Leandro, CA). For the internal control of 8 M urea/5% SDS fraction, 1 μg protein were dot blotted to PVDF membrane and stained with Ponceau S staining (Rane et al., 2004). Statistical analyses were conducted using the two-tailed Student's *t*-test with total of four samples for each group.

For the immunoprecipitation, half of the brain (for hWT/gad) or midbrain region (for L-hI93M/gad) were homogenized in 2 ml ice-cold modified RIPA buffer (50 mM Tris–HCl, pH 7.4; 1% (w/v) Nonidet P40; 0.25% sodium deoxycholate; 150 mM NaCl; 1 mM EDTA) with Complete EDTA-Free Protease Inhibitors and centrifuged at 16,000 × *g* at 4 °C for 20 min. The protein concentration of the resulting supernatants was determined with the Protein Assay Kit (Bio-Rad, Hercules, CA). Immunoprecipitation was performed with a Seize X Mammalian Immunoprecipitation kit (Pierce, Rockford, IL) with some modifications. Briefly, 300 μg of protein was added to a 50 μl slurry of immobilized protein G cross-linked with rabbit polyclonal anti-human UCH-L1 (AB1716; Chemicon, Temecula, CA) or normal rabbit IgG and rotated at 4 °C overnight. The samples were then washed three times with 500 μl of 0.1B buffer (20 mM Tris–HCl, pH 8.0; 0.1 M KCl; 5 mM $MgCl_2$; 10% (w/v) glycerol; 0.1% (w/v) Tween 20; 10 mM β-mercaptoethanol). Elution of samples was performed by adding 20 μl of 5× SDS-PAGE sample buffer, and samples were boiled at 100 °C for 5 min.

2.4. Immunohistochemistry, immunofluorescence and electron microscopy

Brain and peripheral (sciatic) nerve sections from 2-, 7- and 20-week-old mice were analyzed ($n = 3$ for each line) by immunocytochemistry as previously described (Wang et al., 2004; Watanabe et al., 1977) using antibodies to UCH-L1 (1:4000; RA95101, Ultraclone), TH (1:1000; Chemicon) and ubiquitin (1:1000; Sigma–Aldrich, St. Louis, MO). Antibody binding was detected with 3,3′-diaminobenzidine tetrachloride (DAB) or 3-amino-9-ethylcarbazole (AEC) as a peroxidase substrate or Alexa-488- or Alexa-568-conjugated secondary antibodies (Invitrogen, Carlsbad, CA). Sections were then counterstained with hematoxylin. Ultrastructural electron microscopic studies of the substantia nigra were performed as described (Watanabe et al., 1977) using midbrain sections.

2.5. MPTP treatment

For MPTP treatment, the mice received four injections of 30 mg/kg MPTP–HCl intraperitoneally (Research Biochemicals, Natick, MA) in saline at 24-h intervals (Mochizuki et al., 2001).

2.6. Tyrosine hydroxylase-positive cell counting and biochemical analysis

Samples for both histochemistry and biochemical analysis were obtained from the same mouse. Each animal was deeply anesthetized with pentobarbital and perfused transcardially with 10 ml of ice-cold phosphate-buffered saline, and the brain was removed and divided into forebrain and midbrain–hindbrain regions.

For the tyrosine hydroxylase (TH)-positive cell counting, midbrain–hindbrain was fixed with chilled 4% formaldehyde solution (pH 7.4). The procedure of TH-positive cell counting was described previously (Furuya et al., 2004) with minor modifications. Briefly, the substantia nigra was cut into serial sections (30 μm), and every third section was subjected to immunostaining for TH using a polyclonal antibody to TH (a kind gift from I. Nagatsu, Fujita Health University, Aichi, Japan). The Vectorstain Elite ABC kit (Vector Labs, Burlingame, CA) was used for subsequent antibody detection with DAB as a peroxidase substrate. The number of viable TH-positive neurons was assessed by manual counting by a blind observer using coded slides (Furuya et al., 2004). The number of total neuronal cells outside the substantia nigra was counted after Bodian staining in the cerebral cortex (1 mm^2, seven regions per section), cerebellum (total of all lobules) and hippocampus (total number in CA1, CA2, CA3 and dentate gyrus). Statistical analysis were done by one-way ANOVA followed by post hoc test (Fisher's PLSD).

For the biochemical analysis, the striatum was quickly dissected from the forebrain, and the striatal tissue samples were weighed (~30 mg) and homogenized in 10 volumes (w/v) of ice-cold 0.05 M sodium acetate (pH 6.0). Homogenates were centrifuged (18,000 × *g*, 10 min at 4 °C), and the supernatant was frozen immediately on dry ice and stored frozen at −80 °C until use.

For the striatal dopamine measurement, supernatant (50 μl) from the striatal lysate was mixed with an equal volume of 0.2 M perchloric acid containing 0.2 mM EDTA and centrifuged (18,000 × *g*, 10 min at 4 °C), and the supernatant was applied to an HPLC system. Chromatographic separation was achieved using a C18 reversed-phase column (150 mm × 4.6 mm i.d., Model S-100; TOSOH, Tokyo, Japan). The mobile phase (50 mM citrate, 50 mM NaH_2PO_4, 0.1 mM EDTA, 4.36 mM 1-heptanesulfonate, 2.35% acetonitrile, 5.72% MeOH, pH 2.5) was pumped through the chromatographic system at a rate of 1.0 ml/min. A Coulochem electrode array system (ESA Inc., MA) with eight coulometric electrodes was used to quantify the eluted catecholamines and their metabolites. Statistical analysis was done by one-way ANOVA followed by post hoc test (Fisher's PLSD).

TH activity was assayed following the method of Hooper (1997) with minor modifications (Hooper et al., 1997; Naoi et al., 1988). The incubation mixture contained 50 μl of diluted sample and included the following components in a total volume of 200 μl: 0.2 M sodium acetate (pH 6.0), 0.2 M glycerol, 20,000 U/ml catalase, 1.0 mM 6-MPH4, 4.0 U/ml dihydropteridine reductase, 1 mM NADPH and 200 μM L-tyrosine. Incubations were carried out at 37 °C for 10 min in a shaking water bath. Reactions were terminated by adding 600 μl of ice-cold 0.33 M perchloric acid, 17 mM EDTA including 50 pmol of α-methyl DOPA as the internal standard. The L-DOPA produced was extracted onto alumina, and the catechols were eluted with 0.16 M acetic acid followed by 0.02 M phosphoric acid. A sample incubated on ice instead of 37 °C was used as a blank. The amount of L-DOPA was quantified with the HPLC system, as mentioned above. Statistical analysis was done by one-way ANOVA.

2.7. Silver staining

Sixty-micrometer brain sections from 12-week-old mice ($n = 3$ for each group) were stained using FD NeuroSilver kit (FD Neuro-Technologies, Catonsville, MD) according to the manufacturer's protocol to detect argyrophilic grain-positive degenerating neurons.

2.8. Behavioral tests

H-hI93M mice and non-Tg littermates were used for all behavioral analyses. For the accelerated rota-rod test, 20–25-week-old mice were placed on the rod (Ohara, Japan) at a speed of 5 rpm, and the speed was accelerated to 50 rpm in 5 min. The length of time that each mouse was able to remain on the rod before falling was recorded. For the locomotor activity test, 11–13-week-old or 20–23-week-old mice were placed separately in a home cage 4 days before the beginning of analysis for habituation. Two to four mice were monitored at once for locomotor activity on the home cage monitor (Ohara, Japan) for 63 h beginning from 5:30 p.m. All mice were housed with a 12 h light/dark cycle, with the light cycle beginning at 8 a.m. The last 12 h of active night were used for the analysis. Mice were weighed after the analysis; there were no differences between the weights H-hI93M and non-Tg mice (data not shown). Statistical analyses were conducted using the two-tailed Student's *t*-test.

3. Results

3.1. Generation of transgenic mice expressing human *UCHL1*^{I93M} in neurons of the substantia nigra

The human *PDGF-B* promoter was used to drive expression of the human *UCHL1* in Tg mice (Fig. 1A) (Sasahara et al., 1991). Germline transmission of *hUCHL1*^{I93M} was obtained in two independent Tg mouse lines (denoted L-hI93M and H-hI93M, where L and H denote low and high expression, respectively). Germline transmission of *hUCHL1*^{WT} was obtained in one Tg mouse line (denoted hWT). The levels of transgenic mRNA and endogenous *Uchl1* mRNA were assessed by quantitative RT-PCR using primers designed to amplify specifically the *UCHL1* transgene and mouse *Uchl1*, respectively. The estimated relative expression of *UCHL1* among the transgenic lines was H-hI93M > hWT > L-hI93M. The ratio of endogenous mouse *Uchl1* transcripts to transgenic human *UCHL1* transcripts was 111 in H-hI93M, 739 in hWT and 6015 in L-hI93M ($n = 3$ for each line).

At the amino acid level, human and mouse UCH-L1 differ at only 11 discrete positions, and endogenous UCH-L1 is one of the most abundant protein in the brain. Therefore, we were not able to make distinction between the exogenous human UCH-L1 and endogenous mouse UCH-L1 in the brains of Tg mice (data not shown) using immunoblotting analysis with several antibodies against human UCH-L1 from different companies (Chemicon; UltraClone; Medac; Biogenesis). To ascertain the expression of transgene product, we used *gad* mice, which lack endogenous UCH-L1 (Saigoh et al., 1999). We mated mice

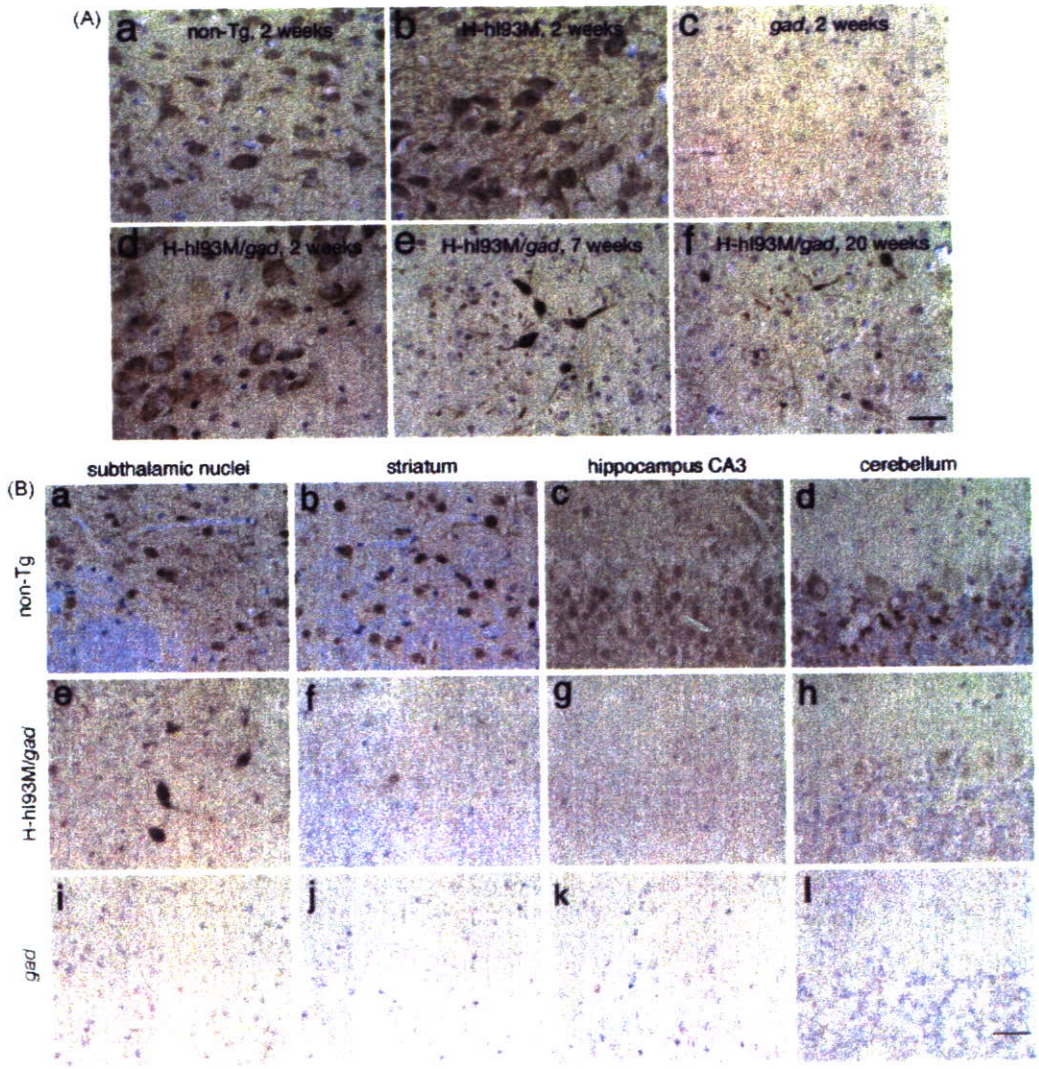

Fig. 2. Immunohistochemistry of UCH-L1 in coronal sections of the substantia nigra (A) and regions outside the substantia nigra (B) in H-hI93M, H-hI93M/*gad* and non-Tg mice. (A) Non-Tg mice (a), H-hI93M mice on a C57BL/6J background (b) and *gad* mice (c) at 2 weeks of age and H-hI93M/*gad* mice at 2 weeks (d), 7 weeks (e) and 20 weeks (f) of age. Neurons expressing UCH-L1 in the substantia nigra decreased in number and area, and densely stained neurons were observed in the aged substantia nigra. Scale bar: 30 μm. (B) UCH-L1 immunohistochemistry of coronal sections at the level of the subthalamic nuclei (a, e, i), striatum (b, f, j), hippocampus CA3 (c, g, k) and cerebellum (d, h, l). Upper row (a–d), non-Tg mice; middle row (e–h), H-hI93M/*gad* mice; lower row (i–l), *gad* mice. All mice were examined at 2 weeks of age. Scale bar: 30 μm.

3. Results

3.1. Generation of transgenic mice expressing human $UCHL1^{I93M}$ in neurons of the substantia nigra

The human *PDGF-B* promoter was used to drive expression of the human *UCHL1* in Tg mice (Fig. 1A) (Sasahara et al., 1991). Germline transmission of $hUCHL1^{I93M}$ was obtained in two independent Tg mouse lines (denoted L-hI93M and H-hI93M, where L and H denote low and high expression, respectively). Germline transmission of $hUCHL1^{WT}$ was obtained in one Tg mouse line (denoted hWT). The levels of transgenic mRNA and endogenous *Uchl1* mRNA were assessed by quantitative RT-PCR using primers designed to amplify specifically the *UCHL1* transgene and mouse *Uchl1*, respectively. The estimated relative expression of *UCHL1* among the transgenic lines was H-hI93M > hWT > L-hI93M. The ratio of endogenous mouse *Uchl1* transcripts to transgenic human *UCHL1* transcripts was 111 in H-hI93M, 739 in hWT and 6015 in L-hI93M ($n = 3$ for each line).

At the amino acid level, human and mouse UCH-L1 differ at only 11 discrete positions, and endogenous UCH-L1 is one of the most abundant protein in the brain. Therefore, we were not able to make distinction between the exogenous human UCH-L1 and endogenous mouse UCH-L1 in the brains of Tg mice (data not shown) using immunoblotting analysis with several antibodies against human UCH-L1 from different companies (Chemicon; UltraClone; Medac; Biogenesis). To ascertain the expression of transgene product, we used *gad* mice, which lack endogenous UCH-L1 (Saigoh et al., 1999). We mated mice

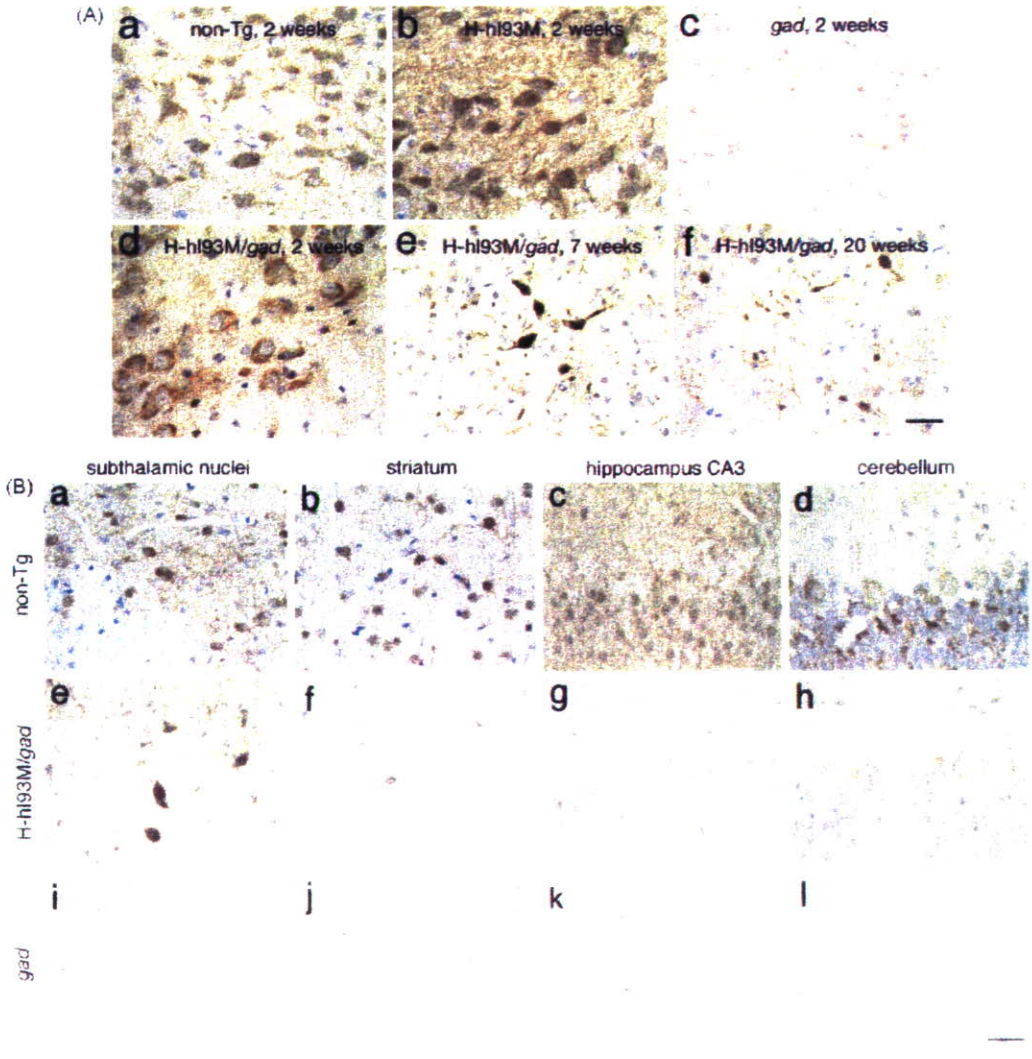

Fig. 2. Immunohistochemistry of UCH-L1 in coronal sections of the substantia nigra (A) and regions outside the substantia nigra (B) in H-hI93M, H-hI93M/*gad* and non-Tg mice. (A) Non-Tg mice (a), H-hI93M mice on a C57BL/6J background (b) and *gad* mice (c) at 2 weeks of age and H-hI93M/*gad* mice at 2 weeks (d), 7 weeks (e) and 20 weeks (f) of age. Neurons expressing UCH-L1 in the substantia nigra decreased in number and area, and densely stained neurons were observed in the aged substantia nigra. Scale bar: 30 μm. (B) UCH-L1 immunohistochemistry of coronal sections at the level of the subthalamic nuclei (a, e, i), striatum (b, f, j), hippocampus CA3 (c, g, k) and cerebellum (d, h, l). Upper row (a–d), non-Tg mice; middle row (e–h), H-hI93M/*gad* mice; lower row (i–l), *gad* mice. All mice were examined at 2 weeks of age. Scale bar: 30 μm.